

## REVIEW

[View Article Online](#)  
[View Journal](#) | [View Issue](#)Cite this: *Chem. Sci.*, 2025, 16, 15836Direct conversion of waste CO<sub>2</sub> over porous polymer catalystsJun-Song Jia,<sup>a</sup> Ying Liang<sup>ID</sup>\*<sup>b</sup> and Ying-Ming Pan<sup>ID</sup>\*<sup>c</sup>

Direct conversion of waste CO<sub>2</sub> avoids CO<sub>2</sub> capture and lowers the cost of CO<sub>2</sub> utilisation; however, this route remains a challenging research topic. Developing catalysts that facilitate the enrichment and conversion of waste CO<sub>2</sub> is therefore essential. Porous polymer catalysts offer unique advantages due to their high surface area and tunable functionality. These materials catalyse the conversion of both simulated waste CO<sub>2</sub> and CO<sub>2</sub> present in industrial waste gases, such as anaerobic fermentation gas, lime kiln waste gas, and coal-fired flue gas. This review summarises recent progress on the direct conversion of waste CO<sub>2</sub> using porous polymer catalysts. It analyses the structural features of these catalysts, their CO<sub>2</sub> adsorption properties, and the associated catalytic mechanisms. A quantitative comparison of catalytic performance—such as turnover frequency, stability, and CO<sub>2</sub> adsorption capacity—is also provided. The findings may support the rational design and synthesis of catalysts for the direct utilisation of waste CO<sub>2</sub>, and provide parameters for the industrialisation of porous polymer catalysts.

Received 23rd June 2025  
Accepted 8th August 2025

DOI: 10.1039/d5sc04590h

[rsc.li/chemical-science](https://rsc.li/chemical-science)

## 1. Introduction

Owing to the continuous development of the global economy and the emission of industrial waste gases, the concentration of CO<sub>2</sub> in the atmosphere has been increasing for centuries.<sup>1–3</sup> As a greenhouse gas, CO<sub>2</sub> can result in many environmental

problems, such as global warming, rising sea levels, the destruction of ecosystems, and extreme weather.<sup>4–6</sup> In recent years, the annual emission of CO<sub>2</sub> into the atmosphere has reached a concerning level of 3.31 billion tons.<sup>7</sup> Therefore, capturing and converting CO<sub>2</sub> to reduce its concentration in the atmosphere are urgent tasks.

CO<sub>2</sub> is a low-cost, safe, non-toxic, and abundant C1 source.<sup>8,9</sup> Its conversion by chemical methods helps reduce CO<sub>2</sub> emissions and yields a range of high value-added products, including synthons, fine chemicals, pharmaceuticals, and hydrocarbon fuels.<sup>10–13</sup> Many methods have been developed to convert CO<sub>2</sub> into bulk chemicals, such as CO, CH<sub>3</sub>OH, and HCOOH.<sup>14,15</sup> CO<sub>2</sub> can also be introduced into organic structures through catalysis to synthesise carboxylic acids, esters, and

<sup>a</sup>College of Chemistry and Environmental Engineering, Key Laboratory of Green Catalysis of Higher Education Institutes of Sichuan, Sichuan University of Science and Engineering, Zigong, 643000, Sichuan, P. R. China

<sup>b</sup>School of Life and Environmental Sciences, Guilin University of Electronic Technology, Guilin 541004, P. R. China. E-mail: [liangyi0774@guet.edu.cn](mailto:liangyi0774@guet.edu.cn)

<sup>c</sup>State Key Laboratory for Chemistry and Molecular Engineering of Medicinal Resources, School of Chemistry and Pharmaceutical Sciences of Guangxi Normal University, Guilin 541004, P. R. China. E-mail: [panym@mailbox.gxnu.edu.cn](mailto:panym@mailbox.gxnu.edu.cn)



Jun-Song Jia

*heterogeneous catalysis.*

Dr Jun-Song Jia received his bachelor's degree from Mianyang Teachers' College. He received his PhD degree from Guangxi Normal University under the guidance of Profs. Ying-Ming Pan and Hai-Tao Tang. He joined the College of Chemistry and Environmental Engineering at Sichuan University of Science and Engineering as a lecturer in 2023. His current research interests focus on transition-metal catalysis and

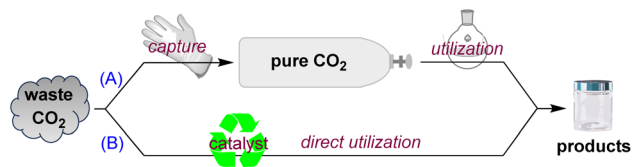


Ying Liang

*methods and instruments.*

Ying Liang is a professor at Guilin University of Electronic Technology. Born on September 11, 1975, in China, she received her BSc degree from Central South University in 1997, followed by an MSc degree from Guangxi University in 2000. She obtained her PhD degree from Xiamen University in 2006. Currently, her research focuses on chemical carbon sequestration and the development of environmental monitoring





Scheme 1 Capture and utilisation of waste CO<sub>2</sub>.

carbonyl compounds.<sup>16–19</sup> However, these reactions require pure CO<sub>2</sub> and generally convert CO<sub>2</sub> under high pressure (Scheme 1A). Currently, the capture of CO<sub>2</sub> from industrial waste gas is usually achieved through liquid or solid adsorption, followed by heating and desorption, and then compression and storage.<sup>20</sup> Desorption and compression require a large amount of energy, resulting in high costs. For example, the cost of capturing one tonne of CO<sub>2</sub> by amine washing is \$59.10 for a typical coal-fired power plant.<sup>21</sup> Therefore, the steps for capture and storage between CO<sub>2</sub> emissions and utilisation must be reduced. If the CO<sub>2</sub> in exhaust gas generated by burning fossil fuels is directly utilised, the steps of capture and storage can be eliminated, thereby reducing the cost of CO<sub>2</sub> utilisation (Scheme 1B).

The exhaust gas emitted from industrial production has a low CO<sub>2</sub> concentration. For example, flue gas contains CO<sub>2</sub> at 10–15 vol%.<sup>20</sup> Anaerobic fermentation gas (AFG) typically consists of CH<sub>4</sub>, CO<sub>2</sub>, N<sub>2</sub>, and H<sub>2</sub>S, with a CO<sub>2</sub> concentration in the range of 30–35 vol%.<sup>22,23</sup> Waste gas from lime kilns mainly comprises N<sub>2</sub>, O<sub>2</sub>, CO<sub>2</sub>, CO, SO<sub>2</sub>, H<sub>2</sub>O, and dust, with a CO<sub>2</sub> concentration of 20–42 vol%.<sup>24–26</sup> In addition, activated CO<sub>2</sub> can be converted into small molecule compounds such as CO and HCOOH.<sup>27–29</sup> In catalytic systems that convert CO<sub>2</sub> into high value-added products, these small molecule products are often overlooked. Therefore, the direct conversion of waste CO<sub>2</sub> faces three challenges: (1) the catalyst must have the capacity for *in situ* enrichment of low-concentration CO<sub>2</sub>; (2) the catalyst must accurately identify CO<sub>2</sub> in exhaust gases without interference from other gas molecules; and (3) selective conversion of CO<sub>2</sub>. Hence, a new catalytic system with enrichment and conversion effects for low-concentration CO<sub>2</sub> must be developed.



Ying-Ming Pan

Ying-Ming Pan is a professor at Guangxi Normal University. He was born in Jiangxi, China. He received his BSc degree from Gannan Normal University and MSc degree from Guangxi University (China). He obtained his PhD degree from Xiamen University in 2010. He was awarded the Mingde Teacher Award in 2018. His present research interests focus on electrochemical synthesis and heterogeneous catalysis.

Porous polymer catalysts are a new class of porous materials with the advantages of high specific surface area, diverse pore structures, low skeleton density, and facile functionalisation.<sup>30–32</sup> They have become versatile hard ligands and carriers for converting many homogeneous catalysts into heterogeneous nano or single-site active-centre catalysts with unique catalytic activity and stability.<sup>33–35</sup> Compared to metal-organic framework (MOF) and covalent organic framework (COF)-based catalysts, polymer catalysts present several advantages: (1) the structure of polymer catalysts is characterised by weak pore uniformity and topological ordering.<sup>36–38</sup> The hierarchical pore structure promotes the physical adsorption of CO<sub>2</sub>. (2) Polymer catalysts are more thermally stable. They are also more stable in water, acid, and base, which broadens their applicability.<sup>37,39</sup> (3) After the loading of metal onto polymer catalysts, the metal is distributed on the surface, facilitating its contact with reactants. The metals within MOFs are typically positioned at the core of the crystal structure, reducing the accessibility of the substrate.<sup>40,41</sup> In addition, porous polymer catalysts have advantages over non-porous catalytic systems: (1) the porous 3D structure increases the catalyst's surface area and allows more active sites to be loaded per unit volume, increasing the probability of CO<sub>2</sub> coming in contact with the catalyst.<sup>30,39</sup> (2) The hierarchical pore structure, especially micropores, contributes to CO<sub>2</sub> enrichment.<sup>42</sup> (3) The swelling properties of porous structures can create a “quasi-homogeneous” catalytic system that accelerates mass transfer and improves catalytic efficiency.<sup>43</sup>

Porous polymer catalysts include porous organic polymers (POPs), porous ionic liquid polymers (PILs), porous organic ligand polymers (POLs), and hypercrosslinked polymers (HCPs).<sup>39</sup> Incorporating active sites that can activate or enrich CO<sub>2</sub> into the framework of porous polymers creates an ideal platform for heterogeneous catalytic CO<sub>2</sub> conversion. Chemists have reviewed the use of porous catalysts for the conversion of pure CO<sub>2</sub>. In 2018, Huang, Liu, and co-workers reviewed the design and synthesis progress of POPs for catalytic CO<sub>2</sub> conversion.<sup>21</sup> The design strategies of these catalysts include nitrogen doping, metallisation, and ionic functionalisation of POPs. In 2022, Wang, Zhou, and co-workers summarised the synthesis of porous PILs and the catalytic details for achieving cycloaddition between pure CO<sub>2</sub> and epoxides.<sup>42</sup> However, only a few reports are available on the enrichment and conversion of CO<sub>2</sub> in exhaust gas catalysed by porous polymers.

In this review, the most recent advances in the design and synthesis of porous polymer catalysts for the conversion of low-concentration CO<sub>2</sub> are summarised. The discussion highlights the synthesis strategies of porous polymers with enrichment effects for low CO<sub>2</sub> concentration and the accurate identification of CO<sub>2</sub> molecules in exhaust gas (simulated exhaust gas). Problems in this field are analysed and future development directions are outlined. This review is divided into two sections: the first addresses simulation of waste CO<sub>2</sub>, and the second addresses real waste CO<sub>2</sub>. Within each section, further categorisation distinguishes waste CO<sub>2</sub> conversion with metal catalysis from that without metal catalysis.



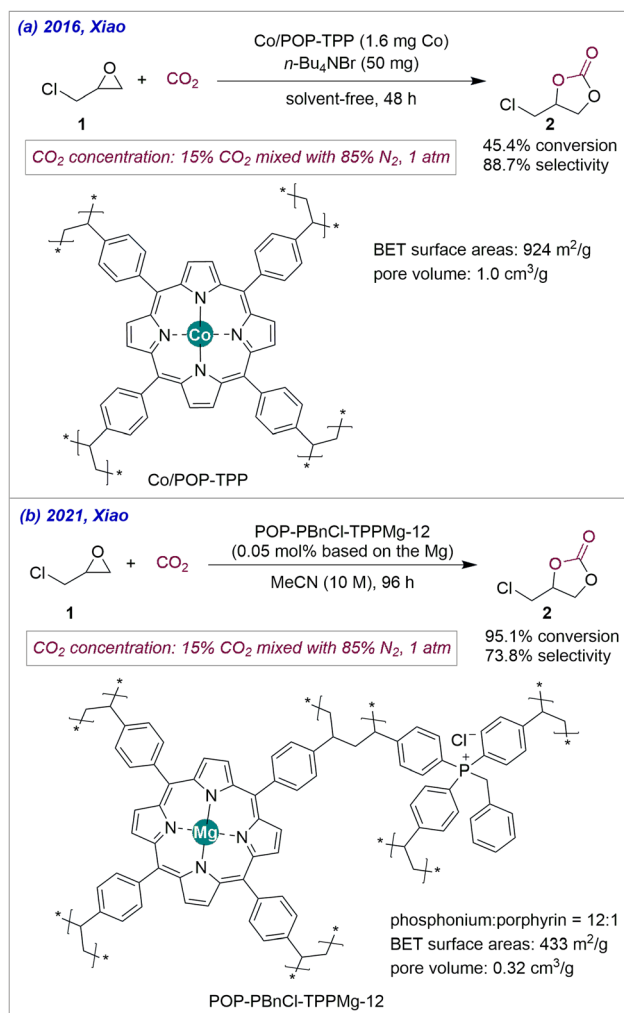
## 2. Direct conversion of simulated waste CO<sub>2</sub>

Simulated waste CO<sub>2</sub> gas is prepared by mixing pure CO<sub>2</sub> with other gases, such as N<sub>2</sub> or air. This mixing process is straightforward and generates a low-concentration CO<sub>2</sub> atmosphere under experimental conditions, facilitating the study of simulated waste CO<sub>2</sub>. Existing reports generally indicate a volume concentration of simulated waste CO<sub>2</sub> of 15–20 vol%, which can represent the CO<sub>2</sub> concentration in actual exhaust gases, such as flue gas or lime kiln gas.<sup>20,24</sup> However, the presence of other gases in waste CO<sub>2</sub> gas cannot be fully replicated by simulating the waste CO<sub>2</sub> gas alone.

### 2.1 Direct conversion of simulated waste CO<sub>2</sub> involving metals

Porous polymer catalysts used to convert waste CO<sub>2</sub> typically contain alkaline sites, which can be loaded with metals to produce metal-loaded porous polymer catalysts. The alkaline sites in these catalysts can alter the electron distribution in CO<sub>2</sub>, facilitating acid–base reactions and thereby activating CO<sub>2</sub>.<sup>21</sup> Additionally, metals loaded onto the catalyst can effectively activate other reaction substrates. The reaction between CO<sub>2</sub> and epoxides to form cyclic carbonates, which achieves 100% atom economy, has received broad attention.<sup>44,45</sup> Numerous heterogeneous catalysts have been developed for the reaction of CO<sub>2</sub> with epoxides to generate cyclic carbonates; however, these catalysts often have drawbacks, such as harsh reaction conditions, catalyst loss, and the need to add large quantities of soluble cocatalysts.<sup>46</sup>

Porphyrins are a class of conjugated macrocyclic structures with 18 $\pi$  electron systems, which enable strong interactions with CO<sub>2</sub>.<sup>47</sup> Furthermore, the cavity structure of porphyrin-based polymers can coordinate with metals to facilitate their loading. Therefore, many porphyrin-based porous materials have been used to convert pure CO<sub>2</sub>. In 2016, Xiao, Meng, and co-workers utilised porphyrin POP loaded with Co<sup>3+</sup> to synthesise a heterogeneous catalyst, Co/POP-TPP, which enabled the reaction of low-concentration CO<sub>2</sub> (15 vol%) with epichlorohydrin **1** by cycloaddition, yielding cyclic carbonates **2** with a 45.4% conversion rate and 88.7% selectivity (Scheme 2a).<sup>48</sup> The catalytic system required the addition of tetrabutylammonium bromide (TBAB) as a cocatalyst. The study found that the activity of the heterogeneous Co/POP-TPP catalyst exceeded that of the corresponding homogeneous Co/TPP catalyst. This difference can be attributed to the strong adsorption capacity of Co/POP-TPP for 15 vol% CO<sub>2</sub> (adsorption capacity of 8 cm<sup>3</sup> g<sup>−1</sup>), whereas the nonporous Co/TPP showed negligible CO<sub>2</sub> adsorption. Activation of the adsorbed CO<sub>2</sub> can be attributed to two factors: the acid–base interaction between nitrogen atoms in porphyrins and CO<sub>2</sub>, and the strong interaction between the porphyrin  $\pi$  system and CO<sub>2</sub>. This catalyst can convert low concentrations of CO<sub>2</sub> at 1 atm and room temperature, which is relevant for utilising CO<sub>2</sub> generated during industrial processes. Although the catalyst successfully



Scheme 2 Co and Mg/porphyrin ligand polymers catalyse the conversion of low-concentration CO<sub>2</sub>.

enabled the conversion of simulated waste CO<sub>2</sub>, the product yield remained relatively low.

In the cycloaddition reaction between epoxides and CO<sub>2</sub>, it is customary to add metal ions or halide anions, both of which serve to activate the substrate.<sup>21</sup> Therefore, the design and synthesis of porous polymer catalysts containing both metal ions and halogen anions will contribute to the conversion of waste CO<sub>2</sub>. In 2021, Xiao's group continued to investigate and synthesise heterogeneous catalysts with multiple synergistic active sites to address the challenge of adding large quantities of soluble cocatalyst TBAB, as shown in Scheme 2a.<sup>46</sup> They prepared a porous organic catalyst, POP-PBnCl-TPPMg-*x*, containing both Lewis acidic and Lewis basic active sites, by copolymerising different proportions of Mg–porphyrin monomers and phosphonium salt monomers (Scheme 2b). Among these, the catalyst POP-PBnCl-TPPMg-12 catalysed the cycloaddition of 15 vol% CO<sub>2</sub> with epoxides to form cyclic carbonates with a 95.1% conversion rate and 73.8% selectivity.

In general, increasing the surface area of polymer catalysts is considered beneficial for enhancing reactant accessibility to



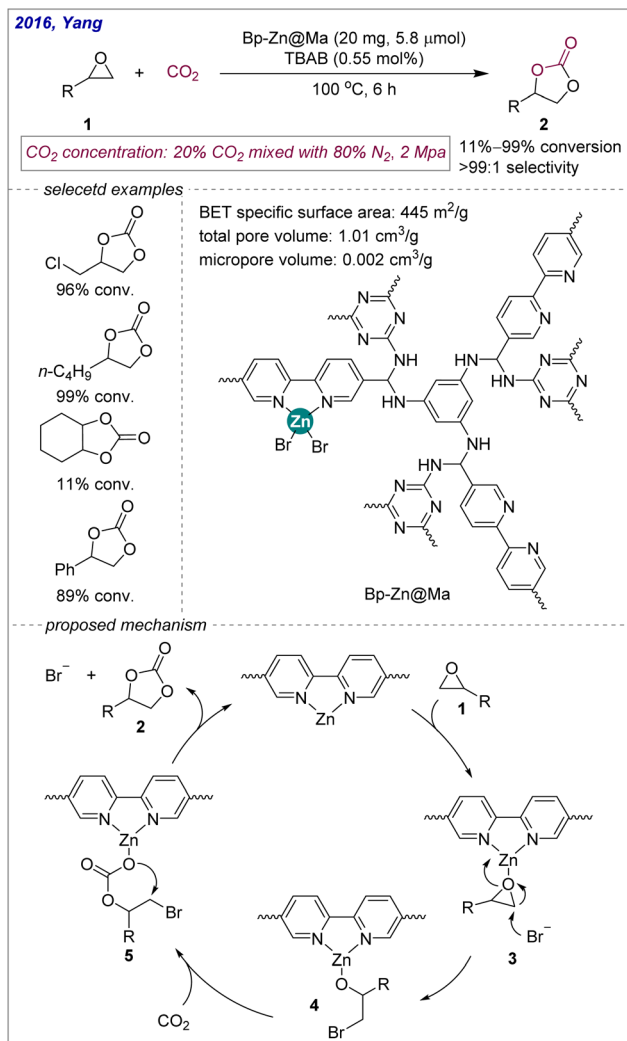
active sites.<sup>21</sup> However, the results from the Co/POM-TPP and POP-PBnCl-TPPMg-12 studies suggest that the Brunauer–Emmett–Teller (BET) surface area and pore volume are not the determining factors in waste CO<sub>2</sub> conversion. Halogen anions integrated onto polymers provide improved cocatalytic effects, likely owing to better dispersion of halogens on the polymer. Additionally, POP-PBnCl-TPPMg-12 does not require cocatalysts and offers a broad range of parameters for converting low-concentration CO<sub>2</sub>. The use of MeCN as a solvent in the catalytic system significantly increased the cyclic carbonate yield, although the mechanism underlying this enhancement was not explained by the authors.

The disordered hierarchical pore structure is a prominent feature of porous polymer catalysts. Pore structures of varying volumes in polymers may serve different functions in the conversion of waste CO<sub>2</sub>. In 2016, Yang, Li, and co-workers prepared a hierarchical meso/microporous polymer catalyst containing a 2,2'-bipyridine Zn(II) coordination structure, Bp-Zn@MA (Scheme 3).<sup>49</sup> When TBAB was used as a cocatalyst,

Bp-Zn@MA catalysed the cycloaddition reaction of simulated flue gas (20 vol% CO<sub>2</sub>) and epoxide to produce cyclic carbonates 2. The N<sub>2</sub> adsorption test showed that the micropore volume of Bp-Zn@MA was 0.002 cm<sup>3</sup> g<sup>-1</sup>, representing 0.198% of the total pore volume. The authors verified, using Henry's law and ideal adsorption solution theory, that Bp-Zn@MA exhibits higher adsorption selectivity for CO<sub>2</sub> than N<sub>2</sub> in mixed gases. Notably, the micropores and abundant N sites in Bp-Zn@MA show selective adsorption for CO<sub>2</sub> in CO<sub>2</sub>/N<sub>2</sub> mixed gases, whereas the role of mesopores is to facilitate the rapid diffusion of reactants and products. Therefore, micropores exert a more pronounced enrichment effect on waste CO<sub>2</sub>. However, the "division of labour" mechanism between micropores and mesopores in catalysis requires further investigation.

In parallel, the authors proposed a mechanism for this reaction. The catalytic cycle begins with the coordination of epoxyethane compounds with zinc to produce compound 3. Bromide anions then perform a nucleophilic attack on epoxyethane to generate Zn-coordinated ring-opening intermediate 4, which combines with CO<sub>2</sub> to afford zinc carbonate species 5. Finally, the intramolecular cyclisation of zinc carbonate species generates the final product 2 and releases bromide anions and regenerated catalyst Bp-Zn@MA, thus completing the catalytic cycle. In this process, zinc activates epoxides, whereas the activation of CO<sub>2</sub> is mainly due to the acid–base interaction between the alkaline N site and CO<sub>2</sub>. Unfortunately, the reaction conditions are harsh (high temperature and pressure) and not suitable for large-scale catalyst application. In addition, the catalytic efficiency decreases when the reaction is carried out in a mixed gas at atmospheric pressure.

Nitrogen heterocyclic carbene (NHC) ligands contain multiple nitrogen atoms that can interact with the carbon in CO<sub>2</sub> to activate it. NHC polymer catalysts also exhibit stronger alkalinity than N-doped polymers, facilitating acid–base interactions with CO<sub>2</sub>.<sup>21</sup> PILs combine the advantages of porous materials, polymers, and ionic liquids, and have shown promise in CO<sub>2</sub> fixation by cycloaddition.<sup>42</sup> PILs synthesised from NHC ligand polymers demonstrate excellent catalytic performance in the conversion of low-concentration CO<sub>2</sub>.<sup>50–54</sup> In 2024, the Liu group prepared a poly(ionic liquid)@porous carbon nanocomposite (PIL-Br<sub>x</sub>@Zn-CTM) through the pyrolysis of fluid precursors and *in situ* polymerisation (Scheme 4).<sup>55</sup> PIL-Br<sub>x</sub>@Zn-CTM contains Lewis acidic (Zn<sup>2+</sup>) and Lewis basic (N) sites and a nucleophilic anion Br<sup>-</sup>. PIL-Br<sub>1.0</sub>@Zn-CTM can absorb low concentrations of CO<sub>2</sub> and catalyse its reaction with epoxides to produce cyclic carbonates 2. The catalytic system does not require cocatalysts or solvents, making it a green approach. In this heterogeneous catalyst, zinc has strong coordination ability, whereas bromide anions have high nucleophilicity. Therefore, the presence of zinc and bromide anions activates epoxides. In addition to the alkaline NHC and N-doped sites, the strong interaction between the large conjugated structure of carbon nanocomposites and CO<sub>2</sub> may also benefit CO<sub>2</sub> adsorption and conversion. However, this catalytic reaction requires a high temperature, which limits its industrial application.

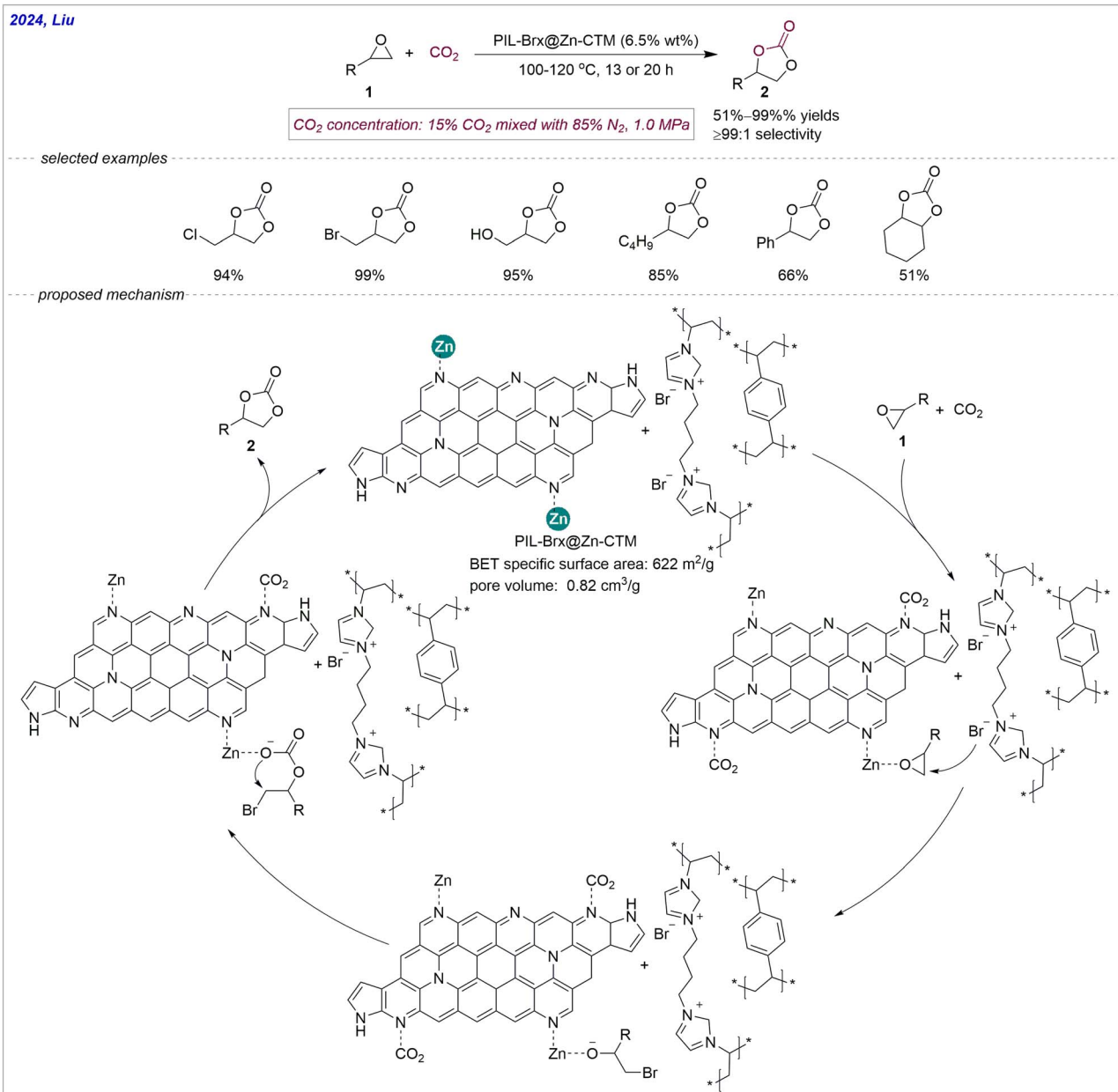


Scheme 3 Bp-Zn@MA catalyzes the conversion of low-concentration CO<sub>2</sub>.





2024, Liu



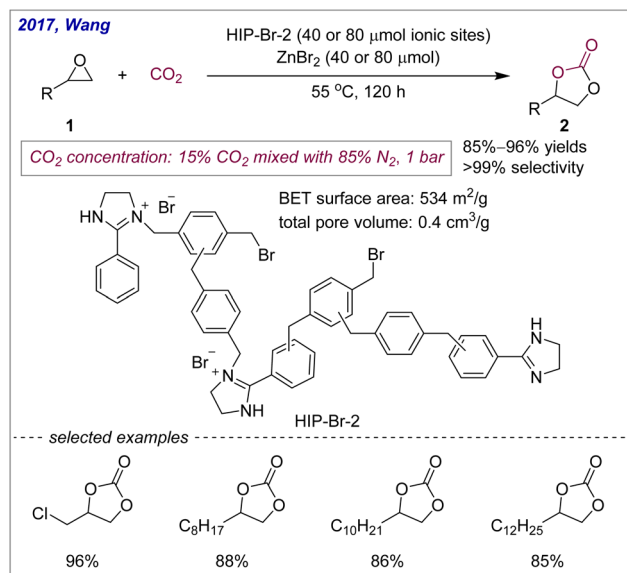
Scheme 4 Poly(ionic liquid)@porous carbon nanocomposites for the capture and *in situ* conversion of low-concentration CO<sub>2</sub>.

The process of PIL-Br<sub>1.0</sub>@Zn-CTM adsorbing and converting low-concentration CO<sub>2</sub> is illustrated in Scheme 4. The alkaline N sites on the catalyst surface adsorb and activate low-concentration CO<sub>2</sub>. Simultaneously, Zn<sup>2+</sup> coordinates with the epoxides **1** and induces C–O bond polarisation. The nucleophilic Br<sup>−</sup> attacks the β-C of epoxyethane, which has minimal steric hindrance, to generate the ring-opening intermediate, which undergoes nucleophilic addition with the CO<sub>2</sub> adsorbed by the catalyst to form alkyl carbonate compounds. Finally, intramolecular cyclisation occurs to generate the final product **2** and release PIL-Br<sub>1.0</sub>@Zn-CTM.

Due to the disorder of the polymer structure, its BET surface area, pore volume, and pore size are difficult to control during preparation. The development of methodologies capable of

precisely modulating the surface area and pore volume of polymers remains a significant challenge in this field. In 2017, Wang, Zhou, and co-workers described the selective capture and conversion of CO<sub>2</sub> from simulated flue gas (15 vol% CO<sub>2</sub>) under mild conditions using imidazolinium-based porous hypercrosslinked ionic polymers (HIPs) with cocatalyst ZnBr<sub>2</sub> (Scheme 5).<sup>56</sup> Notably, the authors adjusted the porosity of HIPs by modifying the initial gel composition. The catalytic effect of this heterogeneous catalyst is substantially better than that of homogeneous ionic liquid monomers and post-modified analogues. The halogen anions in HIPs show high nucleophilicity and high leaving ability, which promote the selective adsorption of CO<sub>2</sub>. Furthermore, the authors propose that HCP exhibits advantages for CO<sub>2</sub> capture and utilisation due to its





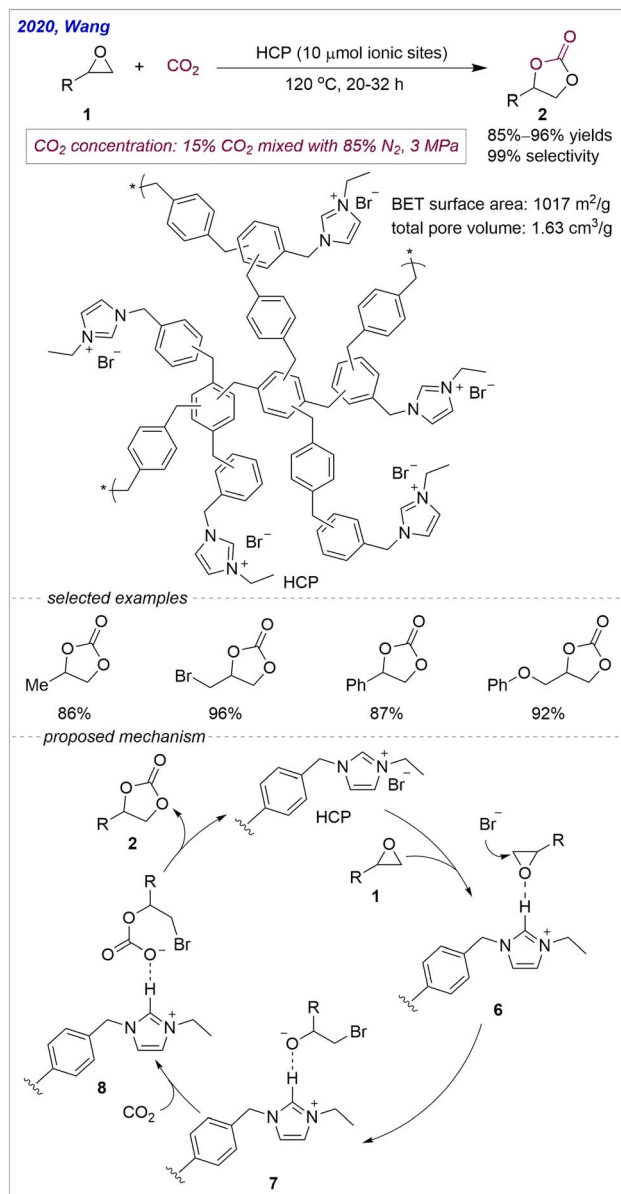
Scheme 5 HIP-Br-2 catalyses the conversion of low-concentration CO<sub>2</sub>.

high surface area and narrowly dispersed micropores. The CO<sub>2</sub> conversion mechanism is the same as for Scheme 3. In addition to halide anions, the alkalinity of NHCs contributes to CO<sub>2</sub> activation. Zn<sup>2+</sup> assists in epoxide activation.

## 2.2 Direct conversion of simulated waste CO<sub>2</sub> without metals

As previously stated, metals and halogens primarily facilitate the activation of epoxides in the conversion of waste CO<sub>2</sub>. The enrichment and transformation of CO<sub>2</sub> depend mainly on the pore structure and alkaline sites of porous polymers. Therefore, within heterogeneous catalytic systems, the reaction between waste CO<sub>2</sub> and epoxides can be achieved without the involvement of metals. In 2020, Wang, Zhou, and co-workers prepared HCPs through Friedel-Crafts alkylation and the conjugate crosslinking of benzyl imidazolium and  $\alpha,\alpha'$ -dichloro-*p*-xylene (DCX) (Scheme 6).<sup>57</sup> Altering the IL : DCX : FeCl<sub>3</sub> ratio changes the BET surface area and total pore volume of the polymer. Notably, the microporous structure and the ionic liquid enhance the enrichment of CO<sub>2</sub> at the active sites. At 273 K and 1 bar, the CO<sub>2</sub> adsorption capacity of HCP is 3.05 mmol g<sup>−1</sup>. HCP can achieve the adsorption and conversion of CO<sub>2</sub> from simulated flue gas (15 vol% CO<sub>2</sub>) without additives or solvents, yielding cyclic carbonates with a turnover number (TON) of 4250–4800. However, this catalytic system requires high temperatures and pressures, which limits its industrial application.

As depicted in Scheme 6, the mechanism of this transformation begins with the formation of hydrogen bonds between the epoxyethane compound 1 and imidazolium salts to afford 6, followed by Br<sup>−</sup> nucleophilic attack on epoxyethane to generate ring-opening products 7. CO<sub>2</sub> insertion into O<sup>−</sup>⋯H then produces opening carbonates 8, which undergo nucleophilic attack to form ring-closing products 2 and release the



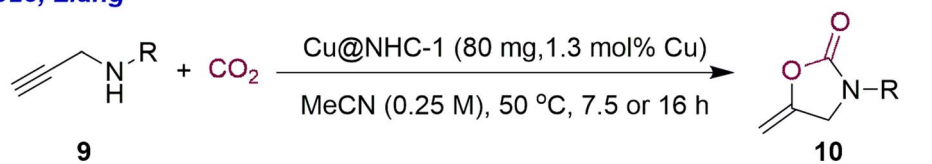
Scheme 6 HCP catalyses the conversion of low-concentration CO<sub>2</sub>.

catalysts. It can be inferred from the mechanism that NHC monomers also activate epoxides. However, the mechanisms of CO<sub>2</sub> adsorption and activation were not clarified by the authors.

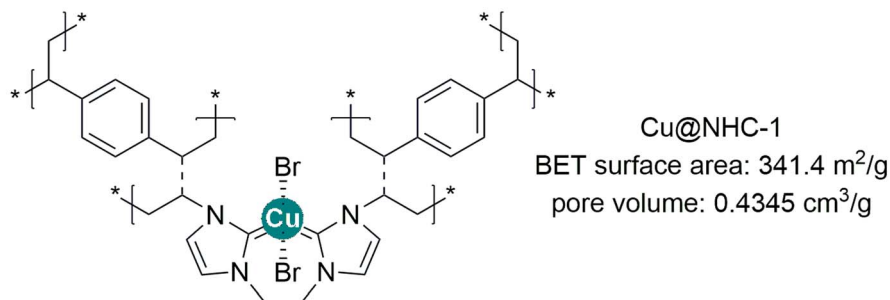
Progress has been made in enriching and converting simulated waste CO<sub>2</sub> using porous polymer catalysts. Some catalysts can achieve the conversion of low-concentration CO<sub>2</sub> at room temperature, atmospheric pressure, and without co-catalysts, confirming the potential of polymer catalysts for industrial waste CO<sub>2</sub> conversion. However, further research is required into the underlying mechanisms of CO<sub>2</sub> enrichment by porous polymer catalysts. In addition, the above waste CO<sub>2</sub> reactions are carried out in closed reactors. Given the fluidity of industrial waste gases, studying the conversion of CO<sub>2</sub> in flowing gases will provide more relevant reference data.



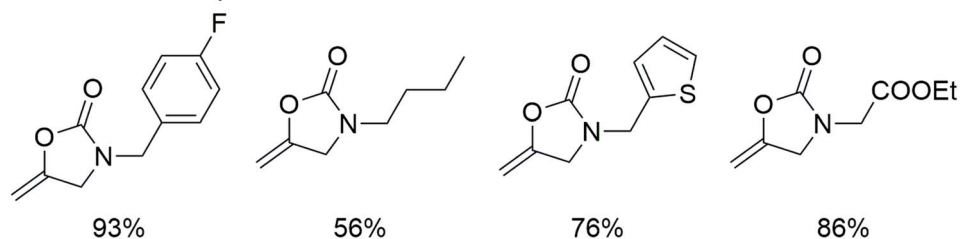
2023, Liang



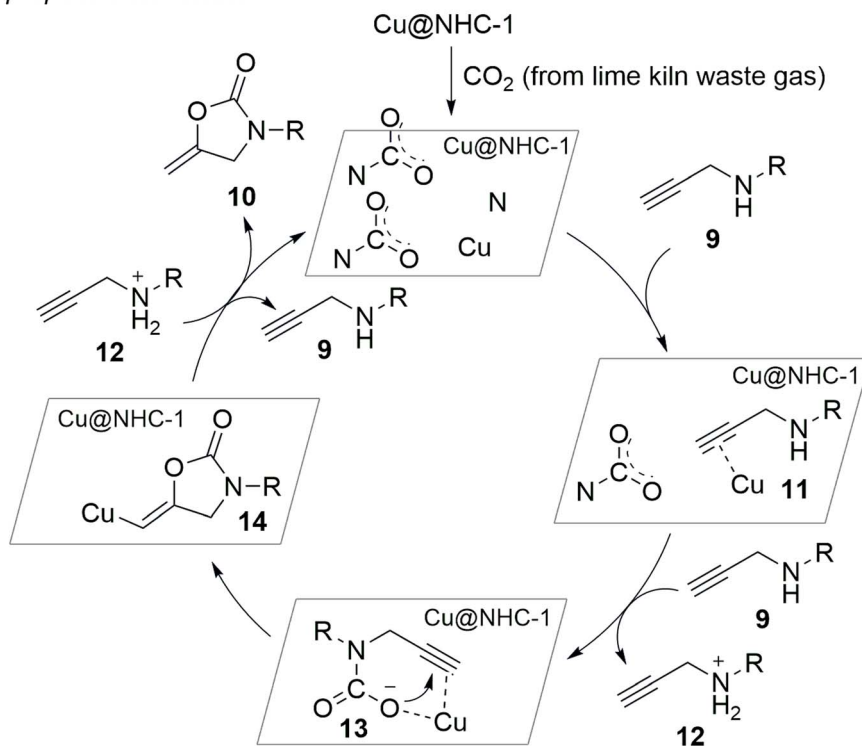
*CO<sub>2</sub> concentration: lime kiln waste gas (67.9% N<sub>2</sub>, 30% CO<sub>2</sub>, 2% O<sub>2</sub>, 0.1% CO, 15 ppm SO<sub>2</sub>, 1 atm)*



selected examples



proposed mechanism

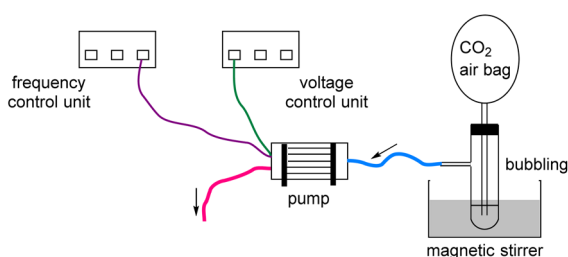
Scheme 7 Cu@NHC-1 catalyses CO<sub>2</sub> conversion in lime kiln waste gas.

### 3. Direct conversion of real waste CO<sub>2</sub>

The flue gas released from industrial production comprises not only waste CO<sub>2</sub> but also other gases, including O<sub>2</sub>, SO<sub>2</sub>, and NO<sub>2</sub>. The presence of these other gases may affect the ability of porous polymer catalysts to capture and convert CO<sub>2</sub>.<sup>58</sup> Therefore, the study of polymer catalysts for the identification and conversion of real waste CO<sub>2</sub> has greater academic and industrial significance. In this section, we review the progress of research into the enrichment and conversion of real waste CO<sub>2</sub> using porous polymer catalysts. The conversion of CO<sub>2</sub> is no longer limited to the cycloaddition with epoxides to form cyclic carbonates, but can also generate a wider range of molecules, such as formamide and oxazolidinone.

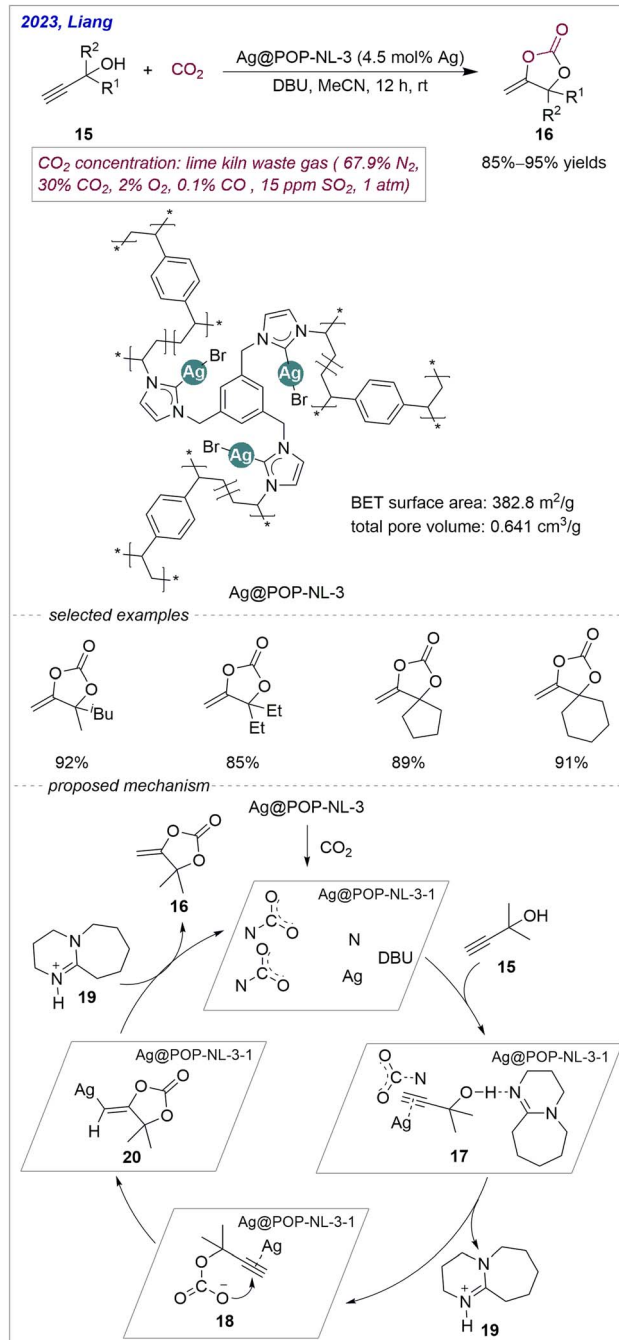
#### 3.1 Direct conversion of real waste CO<sub>2</sub> involving metals

Currently, the enrichment and conversion of CO<sub>2</sub> in exhaust gas are mostly conducted in fixed reaction equipment, so the exhaust gas must first be collected. Directly introducing the exhaust gas into the reaction equipment for the continuous conversion of CO<sub>2</sub> will simplify the production process. In 2023, Liang's group developed the heterogeneous catalyst Cu@NHC-1 for the continuous conversion of CO<sub>2</sub> in lime kiln exhaust gas (30 vol%) using a continuous flow device (Scheme 7).<sup>59</sup> They polymerised a bidentate NHC monomer with divinylbenzene (DVB) to obtain NHC-1, which was coordinated with Cu(OAc)<sub>2</sub> to form Cu@NHC-1 under alkaline conditions. Without co-catalysts, the cyclisation of propargylamine **9** with CO<sub>2</sub> in lime kiln exhaust gas produces oxazolidinones **10**. The catalytic system can also achieve gram-scale conversion (15 mmol). As depicted in Scheme 7, the first step in the reaction mechanism is to use the pore effect of the catalyst and the nucleophilic effect of nitrogen to enrich CO<sub>2</sub>. Meanwhile, propargylamine **9** is captured by the N sites of the catalyst and interacts with the copper centre to form intermediate **11**. The activated CO<sub>2</sub> and propargylamine are converted by cation **12** into aminofomate intermediate **13**, which then undergoes intramolecular cyclisation to form intermediate **14**. Lastly, **14** is protonated by cation **12** to yield the final product oxazolidinone **10**, regenerating the catalyst Cu@NHC-1. Therefore, the NHC in Cu@NHC-1 activates and enriches CO<sub>2</sub>, while copper activates propargylamine. However, the authors did not examine the effects of O<sub>2</sub>, CO, and SO<sub>2</sub> on the enrichment of CO<sub>2</sub> by the polymer.



**Scheme 8** Schematic diagram of the bubbling device for continuous gas flow.

As shown in Scheme 8, a continuous flow device introduces 30 vol% CO<sub>2</sub> into a heterogeneous catalytic system *via* bubbling. Under analogous conditions, the continuous flow apparatus achieves a product yield of 96%, whereas the fixed reactor yields 72%. The authors suggest that the observed difference in yield results from more effective contact between the waste CO<sub>2</sub>, the catalyst, and the substrate in the continuous flow device. This finding highlights the potential application of the catalyst for CO<sub>2</sub> enrichment and conversion in industrial waste gas. However, the authors did not explore the mechanism of



**Scheme 9** Ag@POP-NL-3 catalyses CO<sub>2</sub> conversion in lime kiln waste gas.





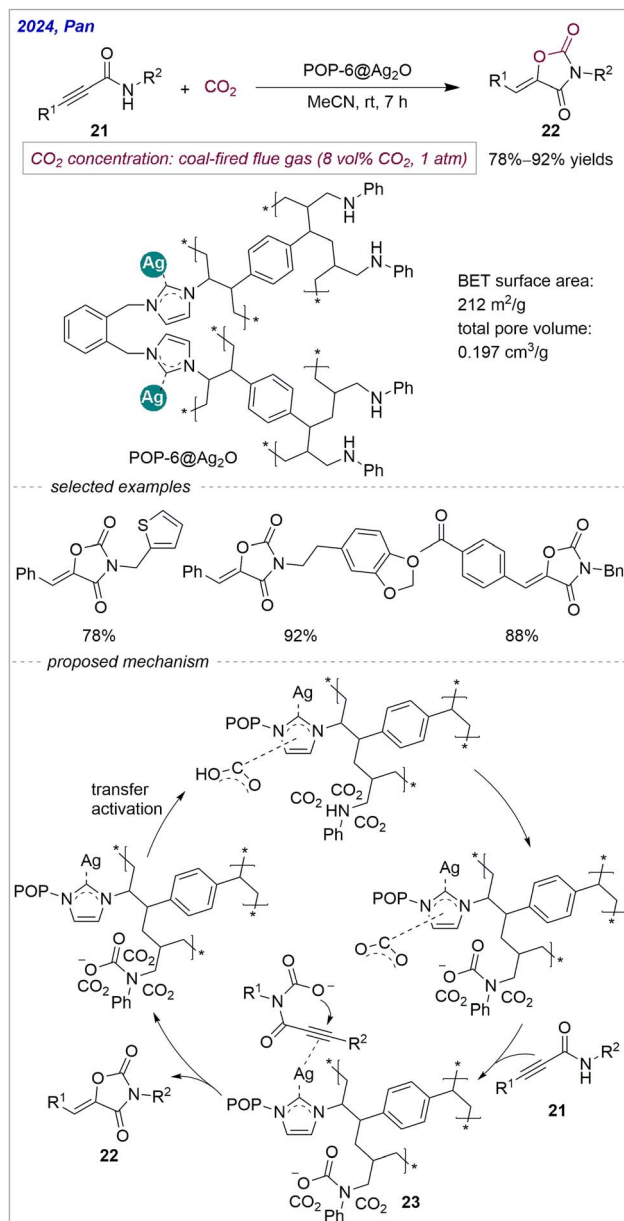
selective adsorption and enrichment of CO<sub>2</sub> in lime kiln exhaust gas by the hierarchical pore structure of the catalyst.

Increasing the number of NHC and metal sites in the monomer enhances the probability of CO<sub>2</sub> contacting active sites, thereby improving the conversion efficiency. In 2023, Liang, Pan and co-workers synthesised the nanocatalyst Ag@POP-NL-3 by pre-coordination and polymerisation of a tridentate NHC monomer with AgNO<sub>3</sub> (Scheme 9).<sup>60</sup> Coordinating before polymerising ensures uniform distribution of Ag on POP-NL-3 and improves catalytic efficiency. The hierarchical pore structure and abundant nitrogen sites of the catalyst guarantee the adsorption and conversion of CO<sub>2</sub>. Using Ag@POP-NL-3 as the heterogeneous catalyst and 0.6 equivalent of DBU as an additive, CO<sub>2</sub> (30 vol%) in lime kiln waste gas reacts with propargyl alcohol **15** to form cyclic carbonates **16**. Raman spectroscopy detected the stretching vibration (1183 cm<sup>-1</sup>) and antisymmetric stretching (2211 cm<sup>-1</sup>) of the N-CO<sub>2</sub> structure. This result confirms the adsorption and activation of CO<sub>2</sub> by N species within the polymer.

Following the addition of Ag@POP-NL-3 to propargylic alcohol, the <sup>1</sup>H nuclear magnetic resonance absorption peak signal of propargylic alcohol decreased, indicating that Ag@POP-NL-3 exerts an adsorption effect on the substrate. The mechanism of this reaction is shown in Scheme 9. First, the hierarchical pore structure and abundant nitrogen sites of the catalyst enrich the low-concentration CO<sub>2</sub> to a locally high concentration. DBU and propargylic alcohol **15** then interact through hydrogen bonding, and Ag coordinates with C≡C to form intermediate **17**. The oxygen atom of propargylic alcohol attacks CO<sub>2</sub>, inserting CO<sub>2</sub> and providing intermediate **18** while releasing DBU-H<sup>+</sup> **19**. Intermediate **18** undergoes intramolecular cyclisation with carbonate and C≡C to form intermediate **20**, followed by reaction with **19** to produce cyclic carbonate **16**. Through controlled experiments, the authors demonstrated that DBU activates propargylic alcohol. It is speculated that, as an organic base, DBU may also activate CO<sub>2</sub>. Therefore, exploring the catalytic effect of DBU on this reaction in the absence of polymer catalysts would improve the accuracy of the proposed mechanism.

The addition of nitrogen-containing components and copolymerisation with NHC monomers can effectively increase the alkaline nitrogen sites in the polymer. In 2024, Pan, Liang and co-workers added copolymer allyl aniline to the bidentate NHC ligand to synthesise polymer POP-6 with abundant nitrogen sites, and then loaded it with Ag<sub>2</sub>O to form POP-6@Ag<sub>2</sub>O (Scheme 10).<sup>61</sup> This polymer catalyst enables the cyclisation between CO<sub>2</sub> in coal-fired flue gas (8 vol%) and propargylamides **21** to produce oxazolidine-2,4-diones **22**. The amine groups in the polymer selectively absorb CO<sub>2</sub> from coal-fired flue gas, and imidazole and silver nanoparticles activate CO<sub>2</sub> and propargylamides.

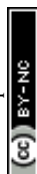
The mechanism of POP-6@Ag<sub>2</sub>O adsorbing and converting waste CO<sub>2</sub> is shown in Scheme 10. The CO<sub>2</sub> in coal-fired flue gas is first adsorbed in the hierarchical pores of the polymer and then onto the amino group. The CO<sub>2</sub> adsorbed by the amine group is transferred to the carbene nitrogen for activation. The nitrogen in propargylamine attacks activated CO<sub>2</sub>, and Ag



Scheme 10 POP-6@Ag<sub>2</sub>O catalyzes CO<sub>2</sub> conversion in coal-fired flue gas.

activates alkynes. Finally, intermediate **23** undergoes intramolecular cyclisation to generate the target product **22**. The enrichment and activation of waste CO<sub>2</sub> with a concentration below 10 vol% in the presence of other gases is a challenging process. The hierarchical porous structure of polymer catalysts facilitates the enrichment of CO<sub>2</sub> and other gases. Therefore, the selectivity of polymers towards waste CO<sub>2</sub> is predominantly attributed to the interaction between the alkaline sites of the polymer and CO<sub>2</sub>. Notably, the stronger alkalinity of aliphatic amines compared to aromatic amines means that integrating alkyl amines into polymer catalysts could improve their ability to enrich and activate waste CO<sub>2</sub>.

More importantly, the authors demonstrated through controlled experiments that neither SO<sub>2</sub> nor NO<sub>2</sub> affects the



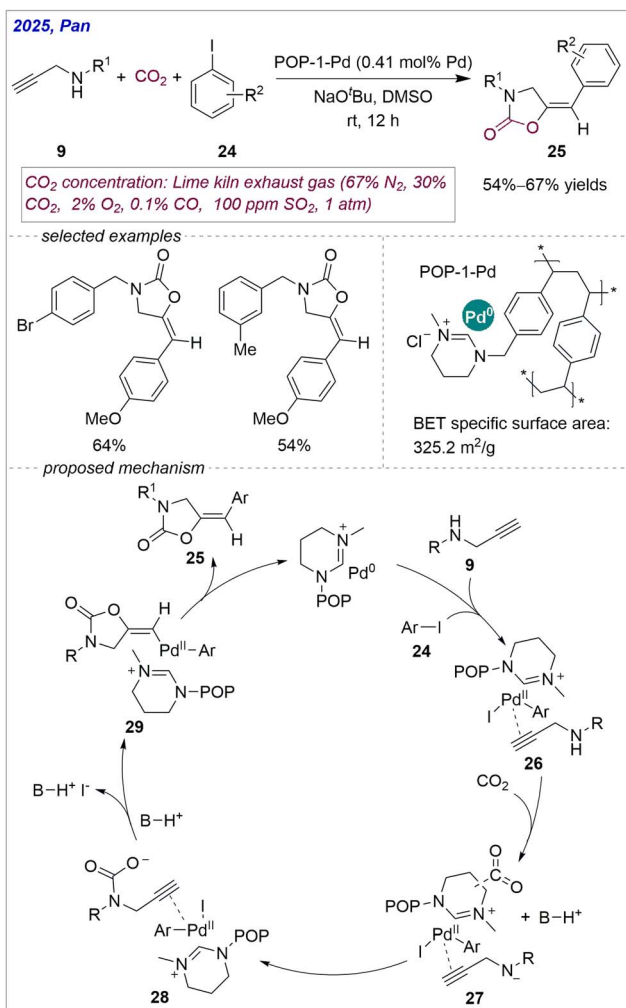
cyclisation reaction. This reaction is unaffected by  $\text{SO}_2$ ,  $\text{NO}_x$  and volatile organic compounds in actual coal-fired flue gas. Therefore, it can be deduced that the presence of other gases in the mixed gas does not affect the catalytic performance of the polymer catalyst. However, the efficiency of the polymer catalyst may decrease as the reaction progresses if the metal loaded on it is sensitive to water and oxygen.

Compared with the two-component reaction involving waste  $\text{CO}_2$ , the three-component reaction is more challenging. In 2025, Pan, Liang and co-workers copolymerised a six-membered NHC monomer with DVB to generate POP-1, which was then loaded with  $\text{Pd}(\text{PPh}_3)_4$  to form the catalyst POP-1-Pd (Scheme 11).<sup>62</sup> At 298.15 K, the  $\text{CO}_2$  adsorption capacity of POP-1-Pd is  $11.62 \text{ m}^3 \text{ g}^{-1}$ . Under the action of  $\text{NaO}^t\text{Bu}$ , POP-1-Pd catalyses a three-component reaction of  $\text{CO}_2$  from lime kiln exhaust gas with propargylamine **9** and aryl iodide **24** to produce oxazolidinone **25**. When  $\text{NHC} : \text{DVB} = 1 : 4$ , the catalyst has the best effect on  $\text{CO}_2$  adsorption and conversion. This finding indicates that the specific surface area of the catalyst has a significant effect on the utilisation of  $\text{CO}_2$ . Moreover, this

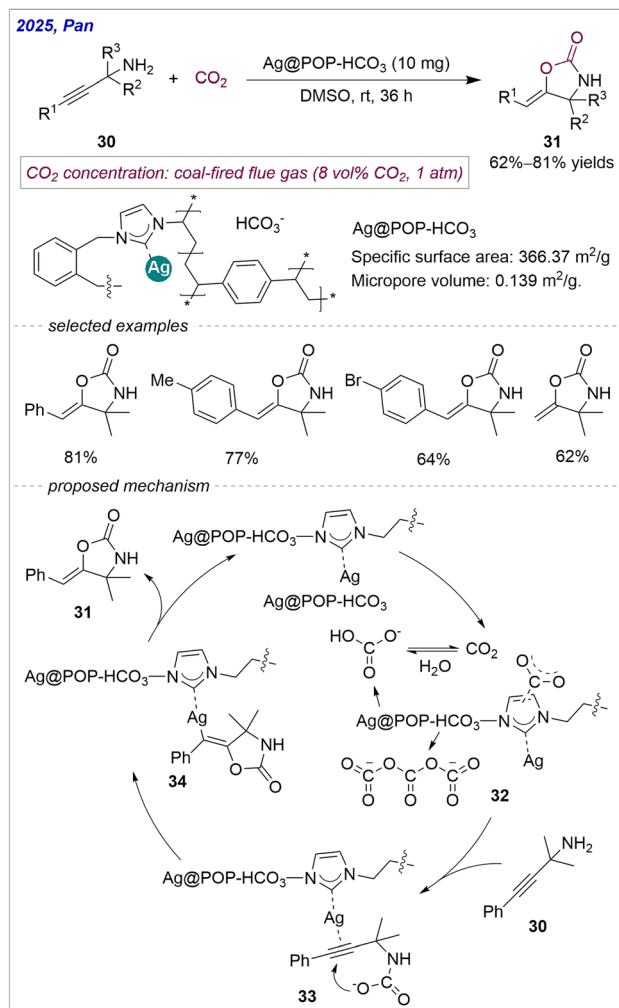
catalytic system can be applied to the gram-level synthesis of oxazolidinone ( $100 \text{ vol}\% \text{ CO}_2$ ,  $1.72 \text{ g}$ ).

$\text{CO}_2$  is enriched near the catalytic sites through the adsorption of imidazolium salts. In parallel,  $\text{Pd}^0$  undergoes oxidative addition with aryl iodide **24** and coordinates with the  $\text{C}\equiv\text{C}$  of propargylamine **9** to form intermediate **26**.  $\text{CO}_2$  is then integrated into intermediate **27** via the imidazole structure. The  $\text{N}^-$  in propargylamine attacks  $\text{CO}_2$  to produce intermediate **28**, which undergoes intramolecular cyclisation to generate intermediate **29**. Finally, **29** undergoes reductive elimination to yield the desired product **25** and regenerate the catalyst. The hierarchical pores of POP-1-Pd provide a microenvironment with increased concentration after adsorbing  $\text{CO}_2$  and substrates. According to the mechanism proposed by the authors, NHC adsorbs and activates waste  $\text{CO}_2$ , while palladium activates iodobenzene and propargylamine. There is no direct interaction between palladium and  $\text{CO}_2$ . Furthermore, the addition of stoichiometric strong base  $\text{NaO}^t\text{Bu}$  renders the reaction conditions harsh.

Interestingly, the anions in the imidazole polymer can be exchanged with other anions, thereby enhancing the ability of



**Scheme 11** POP-1-Pd catalyses  $\text{CO}_2$  conversion in lime kiln exhaust gas.



**Scheme 12** Ag@POP-HCO<sub>3</sub> catalyses  $\text{CO}_2$  conversion in coal-fired flue gas.



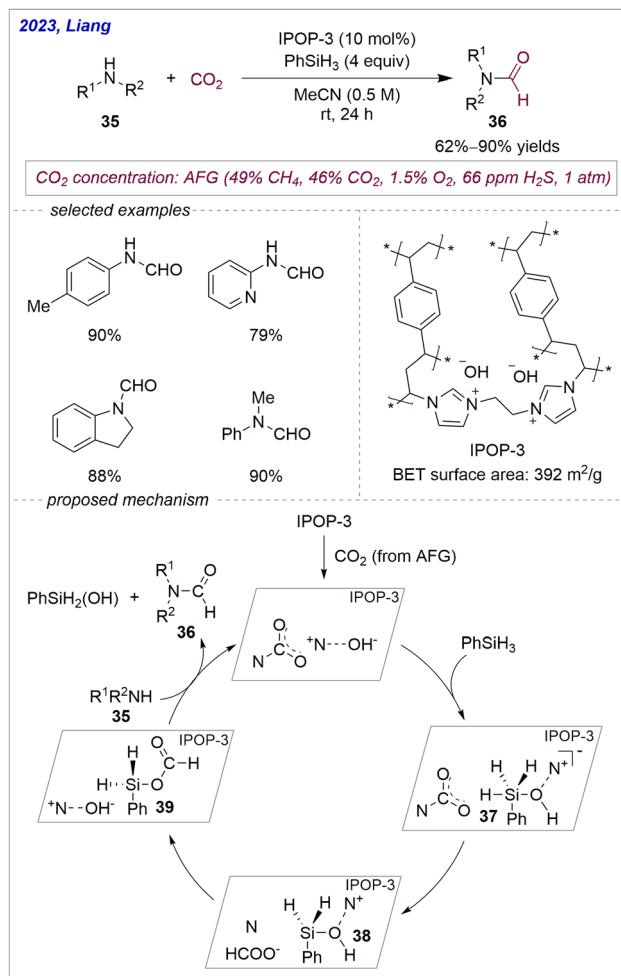
the polymer to enrich and convert waste CO<sub>2</sub>. In 2025, Pan, Liang and co-workers developed an Ag@POP-HCO<sub>3</sub> catalysed reaction of propargylamine **30** with CO<sub>2</sub> in coal-fired flue gas (8 vol%), producing oxazolidinones **31** (Scheme 12).<sup>63</sup> Ag@NHC-HCO<sub>3</sub> can be obtained by modifying the Ag@NHC ligand with HCO<sub>3</sub><sup>−</sup>, which enhances the catalyst's ability to adsorb CO<sub>2</sub>. The specific surface area and micropore volume of the catalyst can be controlled by changing the NHC:HCO<sub>3</sub><sup>−</sup>:DVB ratio. Moreover, the authors designed simulated flue gas with different SO<sub>2</sub> and NO<sub>2</sub> contents. Subsequent controlled experimentation confirmed that SO<sub>2</sub> and NO<sub>2</sub> have no significant effect on the activity of the catalyst.

The mechanism of this conversion is shown in Scheme 12. CO<sub>2</sub> is enriched by the porous structure of polymers and free HCO<sub>3</sub><sup>−</sup> to give **32**. The N-nucleophile of propargylamine then attacks the activated CO<sub>2</sub>, and Ag interacts with C≡C through π electrons to form the carbamate intermediate **33**, followed by intramolecular cyclisation to generate vinyl-silver **34**. Finally, **34** is converted into the final product **31**, and the catalyst Ag@NHC-HCO<sub>3</sub> is regenerated. HCO<sub>3</sub><sup>−</sup> may promote the conversion of waste CO<sub>2</sub> in two ways: (1) as the HCO<sub>3</sub><sup>−</sup> content increases, the specific surface area and microporosity of the catalyst increase, which favours CO<sub>2</sub> adsorption; (2) HCO<sub>3</sub><sup>−</sup> contributes to the formation of the NHC-CO<sub>2</sub> structure between CO<sub>2</sub> and NHC under alkaline conditions.<sup>64,65</sup> According to this mechanism, CO<sub>2</sub> may be converted into other small-molecule compounds, such as H<sub>2</sub>CO<sub>3</sub>. Further analysis of these compounds could clarify the issue of selective CO<sub>2</sub> conversion.

### 3.2 Direct conversion of real waste CO<sub>2</sub> without metals

As demonstrated in the preceding discussion, imidazole polymers and metallised imidazole polymers offer unique advantages in the catalytic conversion of waste CO<sub>2</sub>.<sup>57</sup> CO<sub>2</sub> can undergo C=O bond cleavage, resulting in the formation of CHO fragments. In 2023, Liang, Pan and co-workers reported the enrichment and conversion of CO<sub>2</sub> in AFG (46 vol%) using an ionic NHC ligand polymer, IPOP-3, through metal-free catalysis (Scheme 13).<sup>66</sup> The hydroxide anions, nitrogen sites, and porous structure in IPOP-3 act synergistically to promote the enrichment and conversion of CO<sub>2</sub>. With IPOP-3 as the catalyst and PhSiH<sub>3</sub> as the additive, the primary amines **35** react with the CO<sub>2</sub> present in AFG to produce the corresponding formamide **36**. In addition, this reaction can convert the CO<sub>2</sub> in AFG gas on the gram scale (1.27 g).

As illustrated in Scheme 13, the authors proposed the catalytic cycle. Initially, CO<sub>2</sub> in AFG gas is selectively adsorbed onto IPOP-3 through the combined effect of hydroxide ions, nitrogen sites, and pore channels, creating a local atmosphere of high CO<sub>2</sub> concentration. PhSiH<sub>3</sub> is activated *via* nucleophilic interaction with the OH<sup>−</sup> groups in IPOP-3, forming a high-valence silicon centre **37** that reduces CO<sub>2</sub> to formate anions and intermediate **38**. The formate anion undergoes nucleophilic substitution with intermediate **38** to generate intermediate **39** and regenerate the IPOP-3 catalyst. Finally, amine **35** undergoes nucleophilic substitution with **39** to yield the formamide product **36** and byproduct phenylsilanol. It is evident that waste



Scheme 13 IPOP-3 catalyzes CO<sub>2</sub> conversion in AFG.

CO<sub>2</sub> is also activated by NHC, whereas the reactant amine is not activated by any species. Nevertheless, the use of stoichiometric phenylsilane and the low atomic utilisation rate of CO<sub>2</sub> reduce the atomic economy of this method.

Real waste CO<sub>2</sub> can be directly converted into various high-value-added products using porous polymer catalysis, providing a solution to the environmental problems caused by industrial CO<sub>2</sub> emissions. Although this process is currently at the pilot stage, it provides important information for potential industrial applications. Additionally, the Liang group<sup>59</sup> designed a prototype continuous-flow device for converting waste CO<sub>2</sub>, demonstrating the possibility of directly introducing emitted exhaust gas into a porous polymer catalytic system to achieve selective adsorption and conversion of CO<sub>2</sub>. Designing a comprehensive flow catalytic system and exploring further parameters—including exhaust gas introduction, product separation, catalyst regeneration and circulation, and exhaust gas treatment—will help porous polymer catalysts achieve continuous conversion of waste CO<sub>2</sub> on a large scale. However, there remains a paucity of discussion regarding selectivity in real CO<sub>2</sub> conversion processes.



Table 1 Activities of different catalysts for waste CO<sub>2</sub> conversion

| Catalysts                     | Preparation method           | TOF <sup>a</sup> | Stability/°C | CO <sub>2</sub> adsorption capacity <sup>b</sup>         | Pore sizes/nm  |
|-------------------------------|------------------------------|------------------|--------------|--|----------------|
| Co/POP-TPP                    | Radical polymerization       | 4.4              | 350          | 8 cm <sup>3</sup> g <sup>-1</sup> (15% CO <sub>2</sub> ) | 0.4–2, 12–150  |
| POP-PBnCl-TPPMg               | Copolymerization             | 19.8             | 200          | 50.6 cm <sup>3</sup> g <sup>-1</sup>                     | 0.7–9.3        |
| Bp-Zn@MA                      | Polycondensation             | 21–1580          | 300          | 0.85 mmol g <sup>-1</sup>                                | 1.5, 4–11      |
| PIL-Br <sub>1.0</sub> @Zn-CTM | Pyrolysis and polymerization | 39–72            | 300          | 1.2 mmol g <sup>-1</sup> (0 °C)                          | 3.9 (average)  |
| HIP-Br-2                      | Friedel–Crafts alkylation    | 0.09–0.2         | 300          | 1.9 mmol g <sup>-1</sup>                                 | 0.55–1.61, ~3  |
| HCP                           | Friedel–Crafts alkylation    | 136–240          | 750          | 2.02 mmol g <sup>-1</sup> (0 °C)                         | 6.4 (average)  |
| Cu@NHC-1                      | Copolymerization             | 4–9.6            | 400          | 13.39 cm <sup>3</sup> g <sup>-1</sup>                    | <5             |
| Ag@POP-NL-3                   | Copolymerization             | 1.6–1.8          | 280          | ~10.8 cm <sup>3</sup> g <sup>-1</sup>                    | 50–100         |
| POP-6@Ag <sub>2</sub> O       | Copolymerization             | —                | 350          | 10.5 cm <sup>3</sup> g <sup>-1</sup>                     | 1.85–20.48     |
| POP-1-Pd                      | Copolymerization             | 5.5–6.8          | 300          | 11.62 cm <sup>3</sup> g <sup>-1</sup>                    | 5.87 (average) |
| Ag@NHC–HCO <sub>3</sub>       | Copolymerization             | 81–106           | 400          | ~11.2 cm <sup>3</sup> g <sup>-1</sup>                    | ~3             |
| IPOP-3                        | Copolymerization             | 0.3–0.4          | 250          | 12.3 cm <sup>3</sup> g <sup>-1</sup>                     | ~4             |

| Waste CO <sub>2</sub>                                    | Additives           | T/°C       | t/h       | Conv. or yield % | Selectivity/% | Cycles | Ref. |
|--|---------------------|------------|-----------|------------------|---------------|--------|------|
| 15% CO <sub>2</sub> + 85% N <sub>2</sub> , 1 atm         | TBAB                | 29         | 48        | 45.4             | 88.7          | 18     | 48   |
| 15% CO <sub>2</sub> + 85% N <sub>2</sub> , 1 atm         | —                   | 40         | 96        | 95.1             | 73.8          | 5      | 46   |
| 20% CO <sub>2</sub> + 80% N <sub>2</sub> , 2 Mpa         | TBAB                | 100        | 6         | 11–99            | >99           | 5      | 49   |
| 15% CO <sub>2</sub> + 85% N <sub>2</sub> , 1 Mpa         | —                   | 100 or 120 | 13 or 20  | 51–99            | ≥99           | 7      | 55   |
| 15% CO <sub>2</sub> + 85% N <sub>2</sub> , 1 bar         | ZnBr <sub>2</sub>   | 55         | 120       | 85–96            | >99           | 5      | 56   |
| 15% CO <sub>2</sub> + 85% N <sub>2</sub> , 3 Mpa         | —                   | 120        | 20–32     | 85–96            | 99            | 5      | 57   |
| Lime kiln gas (30% CO <sub>2</sub> ), 1 atm              | —                   | 50         | 7.5 or 16 | 56–94            | —             | 5      | 59   |
| Lime kiln gas (30% CO <sub>2</sub> ), 1 atm              | DBU                 | rt         | 12        | 85–95            | —             | 7      | 60   |
| Coal-fired flue gas (8% CO <sub>2</sub> ), 1 atm         | —                   | rt         | 7         | 78–92            | —             | 6      | 61   |
| Lime kiln gas (30% CO <sub>2</sub> ), 1 atm              | NaO <sup>t</sup> Bu | rt         | 12        | 54–67            | —             | 6      | 62   |
| Coal-fired flue gas (8% CO <sub>2</sub> ), 1 atm         | —                   | rt         | 36        | 62–81            | —             | 3      | 63   |
| Anaerobic fermentation gas (46% CO <sub>2</sub> ), 1 atm | PhSiH <sub>3</sub>  | rt         | 24        | 62–90            | —             | 5      | 66   |

<sup>a</sup> TOF =  $[n(\text{product})]/[n(\text{ionic or metal sites}) \times (\text{reaction time})]$ . <sup>b</sup> Unless indicated otherwise, the term refers to the adsorption capacity for pure CO<sub>2</sub> and 25 °C.

## 4. Summary and outlook

Porous polymer catalysts offer unique advantages for the enrichment and catalytic conversion of waste CO<sub>2</sub>. This review summarises research on the catalytic conversion of waste CO<sub>2</sub>

using porous polymer catalysts. The catalytic efficiency and reaction conditions of different heterogeneous polymer catalysts vary. For clarity, Table 1 provides a summary of the turn-over frequency (TOF), stability, CO<sub>2</sub> adsorption capacity, and reaction conditions involved in the conversion of waste CO<sub>2</sub>. To

Table 2 Gas compositions and experimental conditions

| Waste CO <sub>2</sub> | Waste gas                  | Gas compositions   | Experimental conditions       |                     |         |            |           | Ref. |
|-----------------------|----------------------------|--|-------------------------------|---------------------|---------|------------|-----------|------|
|                       |                            |  | Catalyst                      | Additive            | Solvent | T/°C       | t/h       |      |
| Simulated exhaust gas | —                          | 15% CO <sub>2</sub> + 85% N <sub>2</sub>   | Co/POP-TPP                    | TBAB                | —       | 29         | 48        | 48   |
|                       |                            |  | POP-PBnCl-TPPMg               | —                   | MeCN    | 40         | 96        | 46   |
|                       |                            |  | PIL-Br <sub>1.0</sub> @Zn-CTM | —                   | —       | 100 or 120 | 13 or 20  | 55   |
|                       |                            |  | HIP-Br-2                      | ZnBr <sub>2</sub>   | DMF     | 55         | 120       | 56   |
|                       |                            |  | HCP                           | —                   | —       | 120        | 20–32     | 57   |
|                       |                            |  | Bp-Zn@MA                      | TBAB                | —       | 100        | 6         | 49   |
| Real exhaust gas      | Lime kiln gas              | 20% CO <sub>2</sub> + 80% N <sub>2</sub>   | Cu@NHC-1                      | —                   | MeCN    | 50         | 7.5 or 16 | 59   |
|                       |                            | 67.9% N <sub>2</sub> , 30% CO <sub>2</sub> , 2% O <sub>2</sub> , 0.1% CO, 15 ppm SO <sub>2</sub> | Ag@POP-NL-3                   | DBU                 | MeCN    | rt         | 12        | 60   |
|                       |                            | 67% N <sub>2</sub> , 30% CO <sub>2</sub> , 2% O <sub>2</sub> , 0.1% CO, 100 ppm SO <sub>2</sub>  | POP-1-Pd                      | NaO <sup>t</sup> Bu | DMSO    | rt         | 12        | 62   |
|                       | Coal-fired flue gas        | 8% CO <sub>2</sub>   | POP-6@Ag <sub>2</sub> O       | —                   | MeCN    | rt         | 7         | 61   |
|                       |                            |  | Ag@NHC–HCO <sub>3</sub>       | —                   | DMSO    | rt         | 36        | 63   |
|                       | Anaerobic fermentation gas | 49% CH <sub>4</sub> , 46% CO <sub>2</sub> , 1.5% O <sub>2</sub> , 66 ppm H <sub>2</sub> S        | IPOP-3                        | PhSiH <sub>3</sub>  | MeCN    | rt         | 24        | 66   |







Table 3 A comparison of different porous polymer catalysts

| Porous polymer catalysts                           | Functional groups                                     | Metal incorporation                  | Mechanistic features   | Ref. |
|--|---|--------------------------------------|--|------|
| <b>Porous polymer catalysts loaded with metals</b> |   |                                      |  |      |
| <p>Co/POP-TPP</p>                                  | Porphyrin   | CoCl <sub>2</sub> ·6H <sub>2</sub> O | <ul style="list-style-type: none"> <li>• CO<sub>2</sub> activation mode: the acid–base interaction between nitrogen atoms in porphyrins and CO<sub>2</sub>, and the strong interaction between the porphyrin π system and CO<sub>2</sub></li> <li>• Both cobalt and TBAB activate epichlorohydrins</li> </ul>  | 48   |
| <p>POP-PBnCl-TPPMg</p>                             | Porphyrin and phosphonium salt                        | MgBr <sub>2</sub> ·Et <sub>2</sub> O | <ul style="list-style-type: none"> <li>• CO<sub>2</sub> activation mode: the acid–base interaction between nitrogen atoms in porphyrins and CO<sub>2</sub>, and the strong interaction between the porphyrin π system and CO<sub>2</sub></li> <li>• Both Mg and Cl<sup>−</sup> activate epichlorohydrins</li> </ul>  | 46   |
| <p>Bp-Zn@Ma</p>                                    | 1,3,5-Triazine, bipyridine, and secondary amine group | ZnBr <sub>2</sub>                    | <ul style="list-style-type: none"> <li>• CO<sub>2</sub> activation mode: the acid–base interaction between alkaline N sites and CO<sub>2</sub></li> <li>• Micropores and abundant nitrogen sites selectivity adsorption for CO<sub>2</sub></li> <li>• Mesopores is to facilitate the rapid diffusion of reactants</li> <li>• Both Zn and Br<sup>−</sup> activate epoxides</li> </ul> | 49   |



Table 3 (Contd.)

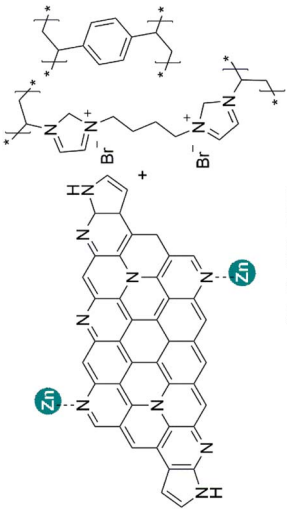
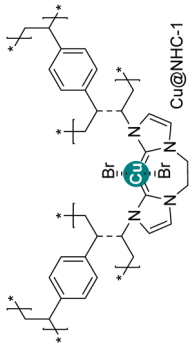
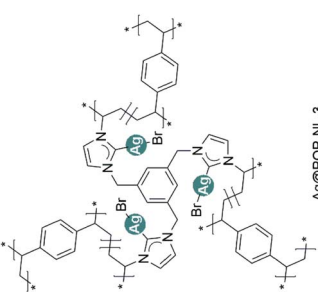
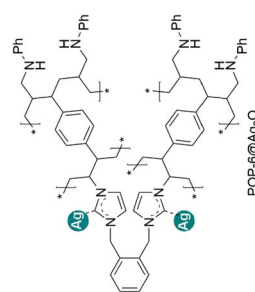
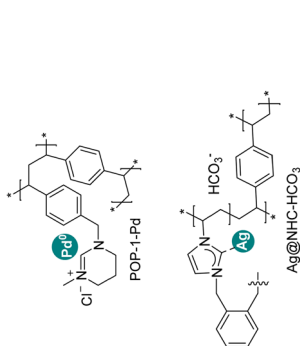
| Porous polymer catalysts   | Functional groups                             | Metal incorporation                      | Mechanistic features   | Ref. |
|--|---|--|--|------|
| <br>PIL-Br <sub>6</sub> @Zn-CTM | Carbon nanocomposite, NHC and Br <sup>−</sup> | Zn(OAc) <sub>2</sub> · 2H <sub>2</sub> O | <ul style="list-style-type: none"> <li>• CO<sub>2</sub> activation mode: the acid–base interactions between CO<sub>2</sub> and NHCs and N-basic sites, as well as a strong interaction between carbon nanocomposites and CO<sub>2</sub></li> <li>• Both Zn and Br<sup>−</sup> activate epoxides</li> </ul> | 55   |
| <br>Cu@NHC-1                    | NHC   | Cu(OAc) <sub>2</sub>                     | <ul style="list-style-type: none"> <li>• CO<sub>2</sub> activation mode: the acid–base interaction between NHCs and CO<sub>2</sub></li> <li>• Cu activates epoxides</li> </ul>   | 59   |
| <br>Ag@POP-NL-3                | NHC and Br <sup>−</sup>                       | AgNO <sub>3</sub>                        | <ul style="list-style-type: none"> <li>• CO<sub>2</sub> activation mode: the acid–base interaction between NHCs and CO<sub>2</sub></li> <li>• Both DBU and Ag activate propargylic alcohols</li> </ul>   | 60   |
| <br>POP-6@Ag <sub>2</sub> O   | NHC and aniline                               | Ag <sub>2</sub> O                        | <ul style="list-style-type: none"> <li>• CO<sub>2</sub> activation mode: the acid–base interactions of CO<sub>2</sub> with NHCs and anilines, respectively</li> <li>• Ag activates propargylamines</li> </ul>  | 61   |

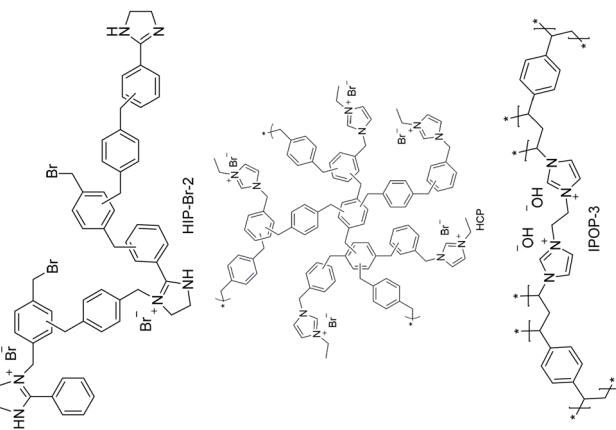


Table 3 (Contd.)

| Functional groups                     | Metal incorporation                | Mechanistic features   | Ref. |
|---------------------------------------|------------------------------------|--|------|
| NHC and Cl <sup>−</sup>               | Pd(PPh <sub>3</sub> ) <sub>4</sub> | <ul style="list-style-type: none"> <li>• CO<sub>2</sub> activation mode: the acid–base interaction between NHCs and CO<sub>2</sub></li> <li>• Pd activates both iodobenzenes and propargylamines</li> </ul>  | 62   |
| NHC and HCO <sub>3</sub> <sup>−</sup> | AgNO <sub>3</sub>                  | <ul style="list-style-type: none"> <li>• CO<sub>2</sub> activation mode: the acid–base interaction between NHCs and CO<sub>2</sub></li> <li>• Ag activates propargylamines</li> <li>• HCO<sub>3</sub><sup>−</sup> promotes NHC–CO<sub>2</sub> formation</li> </ul> | 63   |
| NHC and Br <sup>−</sup>               | ZnBr as the additive               | <ul style="list-style-type: none"> <li>• CO<sub>2</sub> activation mode: the acid–base interaction between NHCs and CO<sub>2</sub></li> <li>• Br<sup>−</sup> activates epoxides</li> </ul>   | 56   |
| NHC and Br <sup>−</sup>               | —                                  | <ul style="list-style-type: none"> <li>• CO<sub>2</sub> activation mode: the acid–base interaction between NHCs and CO<sub>2</sub></li> <li>• Br<sup>−</sup> activates epoxides</li> </ul>   | 57   |
| NHC and OH <sup>−</sup>               | —                                  | <ul style="list-style-type: none"> <li>• CO<sub>2</sub> activation mode: the acid–base interaction between NHCs and CO<sub>2</sub></li> </ul>  | 66   |



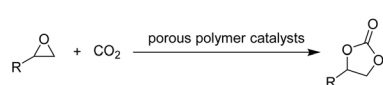
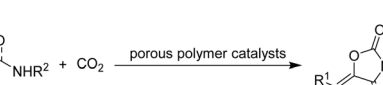
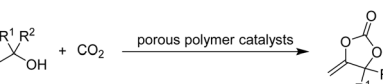
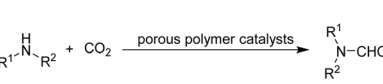
#### Porous polymer catalyst without metal loading



distinguish between “simulated” and “real” waste CO<sub>2</sub>, we have summarised the gas composition and experimental conditions for each type in Table 2. Table 3 summarises the characteristics of the porous polymer catalysts described in this review, including functional groups, metal incorporation, and mechanistic features such as CO<sub>2</sub> activation modes. Moreover, Table 4 summarises the performance of different polymer catalysts in generating the same products (*e.g.* cyclic carbonates, formamides and oxazolidinones), including yield, TOF and selectivity. Our outlook is as follows:

(1) The mechanism of enrichment and activation of waste CO<sub>2</sub> by porous polymer catalysts is as follows: (i) acid–base interactions between active sites and CO<sub>2</sub> can alter the electron distribution of CO<sub>2</sub>; (ii) interactions between specific polymer structures and CO<sub>2</sub>, such as strong interactions observed between conjugated macrocyclic structures and CO<sub>2</sub>; (iii) the hierarchical pore structure of the polymer (primarily micropores) enables CO<sub>2</sub> enrichment, increasing its concentration near catalytic active sites. However, the mechanism of CO<sub>2</sub> enrichment by the pore structure of polymers remains unclear. For mixed gases, the hierarchical pore structure of polymers may enrich each gas molecule. Therefore, further research is required to elucidate the enrichment mechanism of waste CO<sub>2</sub> by the pore structure.

**Table 4** A comparison of the catalytic performance when synthesising the same product

| Catalysts  | Conv. or yield/% | Selectivity/% | TOF      | Ref. |
|--|------------------|---------------|----------|------|
| <p>(a)</p>  |                  |               |          |      |
| Co/POM-TPP   | 45.4             | 88.7          | 4.4      | 48   |
| POP-PBNCI-TPPMg  | 95.1             | 73.8          | 19.8     | 46   |
| Bp-Zn@MA   | 11–99            | >99           | 21–1580  | 49   |
| PIL-Br <sub>1.0</sub> @Zn-CTM  | 51–99            | ≥99           | 39–72    | 55   |
| HIP-Br-2   | 85–96            | >99           | 0.09–0.2 | 56   |
| HCP  | 85–96            | 99            | 136–240  | 57   |
| <p>(b)</p>  |                  |               |          |      |
| Cu@NHC-1   | 56–94            | —             | 4–9.6    | 59   |
| POP-6@Ag <sub>2</sub> O  | 78–92            | —             | —        | 61   |
| POP-1-Pd   | 54–67            | —             | 5.5–6.8  | 62   |
| Ag@POP-HCO <sub>3</sub>  | 62–81            | —             | 81–106   | 63   |
| <p>(c)</p>  |                  |               |          |      |
| Ag@POP-NL-3  | 85–95            | —             | 1.6–1.8  | 60   |
| <p>(d)</p>  |                  |               |          |      |
| IPOP-3   | 62–90            | —             | 0.3–0.4  | 66   |

(2) The BET surface area and total pore volume can be modulated by adjusting the ratio of crosslinking agent to ligand. However, no direct relationship is observed between the BET surface area or total pore volume of the polymer and the conversion of low-concentration CO<sub>2</sub> catalysed by the polymer. Accurately preparing polymer catalysts with specific surface area and pore volume tailored to the size of CO<sub>2</sub> would be more effective for enriching and converting waste CO<sub>2</sub>. In addition, the principle underlying the regulation of BET surface area and total pore volume through the addition of anions requires further investigation.

(3) Some reports using gram-scale reactions indicate that porous polymer catalysts may catalyse the large-scale conversion of waste CO<sub>2</sub>. The development of continuous flow devices demonstrates the feasibility of introducing industrial waste gas directly into the catalytic system for enrichment and conversion of waste CO<sub>2</sub>. To our knowledge, no published studies have demonstrated the use of polymeric catalysts for industrial-scale CO<sub>2</sub> separation and conversion, nor have the economic viability and technical feasibility of such processes been systematically evaluated. Therefore, further research is required to transition catalysts from laboratory to industrial production. Further development of milder and more efficient porous polymer catalysts is required. Sufficient attention should also be given to reactor design and optimisation.

(4) Traditionally, the discovery of catalysts for CO<sub>2</sub> absorption and conversion involves a sequential process of polymer synthesis, catalyst optimisation and extensive data collection. Nevertheless, this empirical trial-and-error approach is not only labour-intensive, but also inherently inefficient. In the context of the rapid advancement of artificial intelligence, data-driven machine learning (ML) approaches can now be used to discover high-performance catalysts through computational prediction, thus eliminating the need for extensive experimental procedures.<sup>67</sup> Therefore, implementing ML-based predictive modelling for catalyst optimisation can significantly reduce the time taken to develop porous polymer catalysts, while ensuring enhanced catalytic efficacy. On the other hand, ML shows great promise in characterising the surface architectures of heterogeneous catalysts using computational modelling techniques such as density functional theory, molecular dynamics and Monte Carlo simulations.<sup>68</sup> As previously established, microstructural parameters of porous polymer catalysts, including pore size distribution, total pore volume and BET-specific surface area, affect the performance of CO<sub>2</sub> capture and enrichment. Consequently, compiling a comprehensive database of these surface characteristics from catalysts reported in the literature is essential for the ML-driven optimisation of porous polymer parameters.

(5) The adsorption outcomes of porous polymer catalysts on waste CO<sub>2</sub> have been detected using FT-IR and Raman spectroscopy.<sup>69</sup> Nevertheless, the dynamic adsorption and conversion process of CO<sub>2</sub> on polymer surfaces remains to be elucidated. In order to facilitate more intuitive detection of the conversion process of low concentration CO<sub>2</sub>, there is a critical research frontier in the development of advanced *in situ*





spectroscopic methodologies capable of real-time monitoring of both selective adsorption and activation phenomena.

(6) In recent years, the development of bifunctional materials (BFMs) for capturing and converting CO<sub>2</sub> has emerged as a significant research area. Typically, BFMs comprise two phases: a catalyst phase and a high-temperature adsorbent phase. Meanwhile, porous polymer catalysts have excellent thermal stability (300–750 °C, Table 1), making them compatible with high-temperature adsorption.<sup>70</sup> Therefore, the integration of porous polymer catalysts with high-temperature adsorption phases, such as CaO, to prepare novel BFMs for CO<sub>2</sub> adsorption and conversion is also worth studying. The good adsorption capabilities of porous polymers for waste CO<sub>2</sub> may facilitate the capture and conversion of CO<sub>2</sub> by BFMs, obviating the necessity for elevated temperature conditions.

(7) Polymer-based membranes exhibit significant advantages in manufacturability and functional versatility, enabling their widespread adoption in liquid/gas separation processes.<sup>71</sup> Notably, porous organic polymers offer superior design flexibility due to their tunable wettability, chemical stability, and facile modification capabilities.<sup>72</sup> These attributes position porous polymer catalysts as promising alternatives to conventional membrane materials—including polydimethylsiloxane, polyvinylidene fluoride, poly(vinyl alcohol), and polyethylene glycol laurate—with demonstrated potential to enhance performance metrics in critical applications ranging from gas separation and osmotic processes to advanced filtration and solvent recovery systems. On the other hand, millimetre-sized composite beads are prepared using a double cross-linking strategy, combining powdered, porous polymer catalysts with additives such as polyacrylic acid, CaCl<sub>2</sub> and sodium alginate.<sup>73</sup> The assembly of fixed-bed catalytic systems utilizing these composite beads as structured packing media has evolved into a burgeoning research focus, particularly for enabling continuous-flow transformation of reactants with enhanced mass transfer efficiency. For gas-phase reaction systems targeting waste CO<sub>2</sub> valorization, continuous gas feeding into the flow reactor configuration enables simultaneous concentration enhancement and catalytic conversion through optimized gas-liquid-solid interfacial contact.

We hope that this review provides a new perspective on the enrichment and conversion of waste CO<sub>2</sub> using porous polymer catalysts and offers direction for the design and synthesis of heterogeneous catalysts that can facilitate more efficient conversion of waste CO<sub>2</sub>.

## Author contributions

All authors contributed to the conceptualization and literature search. J.-S. Jia wrote the first draft and made all schemes. All authors were involved in revising, editing, and proofreading.

## Conflicts of interest

There are no conflicts to declare.

## Data availability

No primary research results, software or code have been included and no new data were generated or analysed as part of this review.

## Acknowledgements

We thank the National Natural Science Foundation of China (No. 22471046, 52170107, and 52360014), the Scientific Research and Innovation Team Program of Sichuan University of Science and Engineering (SUSE652A014), the Chemical Synthesis and Pollution Control Key Laboratory of Sichuan Province (CSPC202408), Sichuan University of Science and Engineering (2023RC10), and the Special Polymer Materials for Automobile Key Laboratory of Sichuan Province (Sichuan University of Arts and Science) (TZGC2024ZB-02) for financial support.

## References

- 1 S. Solomon, G. Plattner, R. Knutti and P. Friedlingstein, *Proc. Natl. Acad. Sci. U. S. A.*, 2009, **106**, 1704–1709.
- 2 G. Singh, J. Lee, A. Karakoti, R. Bahadur, J. Yi, D. Zhao, K. AlBahily and A. Vinu, *Chem. Soc. Rev.*, 2020, **49**, 4360–4404.
- 3 R. L. Tyne, P. H. Barry, M. Lawson, D. J. Byrne, O. Warr, H. Xie, D. J. Hillegonds, M. Formolo, Z. M. Summers, B. Skinner, J. M. Eiler and C. J. Ballentine, *Nature*, 2021, **600**, 670–674.
- 4 Y. Zhou, J. Zhang, L. Wang, X. Cui, X. Liu, S. S. Wong, H. An, N. Yan, J. Xie, C. Yu, P. Zhang, Y. Du, S. Xi, L. Zheng, X. Cao, Y. Wu, Y. Wang, C. Wang, H. Wen, L. Chen, H. Xing and J. Wang, *Science*, 2021, **373**, 315–320.
- 5 P. García-Gutiérrez, R. M. Cuéllar-Franca, D. Reed, G. Dowson, P. Styring and A. Azapagic, *Green Chem.*, 2019, **21**, 4100–4114.
- 6 M. Pera-Titus, *Chem. Rev.*, 2014, **114**, 1413–1492.
- 7 D.-G. Yu and L.-N. He, *Green Chem.*, 2021, **23**, 3499–3501.
- 8 S. Huang, B. Yan, S. Wang and X. Ma, *Chem. Soc. Rev.*, 2015, **44**, 3079–3116.
- 9 E. S. Sanz-Pérez, C. R. Murdock, S. A. Didas and C. W. Jones, *Chem. Rev.*, 2016, **116**, 11840–11876.
- 10 M. He, Y. Sun and B. Han, *Angew. Chem., Int. Ed.*, 2013, **52**, 9620–9633.
- 11 M. D. Burkart, N. Hazari, C. L. Tway and E. L. Zeitler, *ACS Catal.*, 2019, **9**, 7937–7956.
- 12 V. A. Peshkov, O. P. Pereshivko, A. A. Nechaev, A. A. Peshkov and E. V. Van Der Eycken, *Chem. Soc. Rev.*, 2018, **47**, 3861–3898.
- 13 M. Aresta, A. Dibenedetto and A. Angelini, *Chem. Rev.*, 2014, **114**, 1709–1742.
- 14 R. Cauwenbergh and S. Das, *Green Chem.*, 2021, **23**, 2553–2574.
- 15 S. Das, J. Perez-Ramirez, J. Gong, N. Dewangan, K. Hidajat, B. C. Gates and S. Kawi, *Chem. Soc. Rev.*, 2020, **49**, 2937–3004.
- 16 K. Huang, C.-L. Sun and Z.-J. Shi, *Chem. Soc. Rev.*, 2011, **40**, 2435–2452.



- 17 J.-H. Ye, T. Ju, H. Huang, L.-L. Liao and D.-G. Yu, *Acc. Chem. Res.*, 2021, **54**, 2518–2531.
- 18 G.-Q. Sun, L.-L. Liao, C.-K. Ran, J.-H. Ye and D.-G. Yu, *Acc. Chem. Res.*, 2024, **57**, 2728–2745.
- 19 Z. Chen, S. Du, J. Zhang and X.-F. Wu, *Green Chem.*, 2020, **22**, 8169–8182.
- 20 D. Aaron and C. Tsouris, *Sep. Sci. Technol.*, 2005, **40**, 321–348.
- 21 K. Huang, J.-Y. Zhang, F. Liu and S. Dai, *ACS Catal.*, 2018, **8**, 9079–9102.
- 22 A. S. Al-Fatesh, H. atia, A. A. Ibrahim, A. H. Fakeeha, S. K. Singh, N. K. Labhsetwar, H. Shaikh and S. O. Qasim, *Renewable Energy*, 2019, **140**, 658–667.
- 23 S. B. Walker, D. Sun, D. Kidon, A. Siddiqui, A. Kuner, M. Fowler and D. S. A. Simakov, *Int. J. Energy Res.*, 2018, **42**, 1714–1728.
- 24 R. Bouma, F. Vercauteren, P. Van Os, E. Goetheer, D. Berstad and R. Anantharaman, *Energy Procedia*, 2017, **114**, 72–80.
- 25 C. Nwaoha, P. Tontiwachwuthikul and A. Benamor, *J. Environ. Chem. Eng.*, 2018, **6**, 7102–7110.
- 26 Y. Zhang, X. Ji and X. Lu, *Appl. Energy*, 2014, **130**, 237–243.
- 27 A. Álvarez, A. Bansode, A. Urakawa, A. V. Bavykina, T. A. Wezendonk, M. Makkee, J. Gascon and F. Kapteijn, *Chem. Rev.*, 2017, **117**, 9804–9838.
- 28 S.-T. Bai, G. De Smet, Y. Liao, R. Sun, C. Zhou, M. Beller, B. U. Maes and B. F. Sels, *Chem. Soc. Rev.*, 2021, **50**, 4259–4298.
- 29 P. Gao, L. Zhang, S. Li, Z. Zhou and Y. Sun, *ACS Cent. Sci.*, 2020, **6**, 1657–1670.
- 30 Q. Sun and F.-S. Xiao, *Acc. Mater. Res.*, 2022, **3**, 772–781.
- 31 S. Kramer, N. R. Bennedsen and S. Kegnæs, *ACS Catal.*, 2018, **8**, 6961–6982.
- 32 P. Kaur, J. T. Hupp and S. T. Nguyen, *ACS Catal.*, 2011, **1**, 819–835.
- 33 W.-Y. Huang, G.-Q. Wang, W.-H. Li, T.-T. Li, G.-J. Ji, S.-C. Ren, M. Jiang, Y. Li, H.-T. Tang, Y.-M. Pan and Y.-J. Ding, *Chem*, 2020, **6**, 2300–2313.
- 34 J.-S. Jia, J.-R. Luo, W.-H. Li, F.-H. Cui, Y.-M. Pan and H.-T. Tang, *Adv. Sci.*, 2024, **11**, 2308238.
- 35 Y. Zhu, D. Mukherjee, T. R. Helgert and S. T. Nguyen, *CCS Chem.*, 2023, **5**, 445–454.
- 36 S. Dalapati, C. Gu and D. Jiang, *Small*, 2016, **12**, 6513–6527.
- 37 Y.-Y. Zhu, Y.-Y. He, Y.-X. Li, C.-H. Liu and W. Lin, *Chem.-Eur. J.*, 2024, **30**, e202400842.
- 38 M. Asad, M. I. Anwar, A. Abbas, A. Younas, S. Hussain, R. Gao, L.-K. Li, M. Shahid and S. Khan, *Coord. Chem. Rev.*, 2022, **463**, 214539.
- 39 Q. Sun, Z. Dai, X. Meng and F.-S. Xiao, *Chem. Soc. Rev.*, 2015, **44**, 6018–6034.
- 40 S. Daliran, A. R. Oveisi, Y. Peng, A. López-Magano, M. Khajeh, R. Mas-Ballesté, J. Alemán, R. Luque and H. Garcia, *Chem. Soc. Rev.*, 2022, **51**, 7810–7882.
- 41 P. Rani, R. Das and C. M. Nagaraja, *Inorg. Chem. Front.*, 2025, **12**, 430–478.
- 42 G. Li, S. Dong, P. Fu, Q. Yue, Y. Zhou and J. Wang, *Green Chem.*, 2022, **24**, 3433–3460.
- 43 Q. Sun, Z. Dai, X. Liu, N. Sheng, F. Deng, X. Meng and F.-S. Xiao, *J. Am. Chem. Soc.*, 2015, **137**, 5204–5209.
- 44 Q.-W. Song, Z.-H. Zhou and L.-N. He, *Green Chem.*, 2017, **19**, 3707–3728.
- 45 X. -B. Lu and D. J. Darensbourg, *Chem. Soc. Rev.*, 2012, **41**, 1462–1484.
- 46 Z. Dai, Y. Tang, F. Zhang, Y. Xiong, S. Wang, Q. Sun, L. Wang, X. Meng, L. Zhao and F.-S. Xiao, *Chin. J. Catal.*, 2021, **42**, 618–626.
- 47 S. Kumar, M. Y. Wani, C. T. Arranja, J. D. A. e Silva, B. Avula and A. J. Sobral, *J. Mater. Chem. A*, 2015, **3**, 19615–19637.
- 48 Z. Dai, Q. Sun, X. Liu, C. Bian, Q. Wu, S. Pan, L. Wang, X. Meng, F. Deng and F.-S. Xiao, *J. Catal.*, 2016, **338**, 202–209.
- 49 J. Chen, H. Li, M. Zhong and Q. Yang, *Green Chem.*, 2016, **18**, 6493–6500.
- 50 Z. Guo, Y. Hu, S. Dong, L. Chen, L. Ma, Y. Zhou, L. Wang and J. Wang, *Chem Catal.*, 2022, **2**, 519–530.
- 51 Y. He, X. Li, W. Cai, H. Lu, J. Ding, H. Li, H. Wan and G. Guan, *ACS Sustainable Chem. Eng.*, 2021, **9**, 7074–7085.
- 52 X. Wang, Y. Zhou, Z. Guo, G. Chen, J. Li, Y. Shi, Y. Liu and J. Wang, *Chem. Sci.*, 2015, **6**, 6916–6924.
- 53 S. Ghazali-Esfahani, H. Song, E. Păunescu, F. D. Bobbink, H. Liu, Z. Fei, G. Laurenczy, M. Bagherzadeh, N. Yan and P. J. Dyson, *Green Chem.*, 2013, **15**, 1584–1589.
- 54 Y. Xie, J. Liang, Y. Fu, M. Huang, X. Xu, H. Wang, S. Tu and J. Li, *J. Mater. Chem. A*, 2018, **6**, 6660–6666.
- 55 M. Liu, C. Ma, Q. Wang, R. Li, S. Yu, H. Chen and F. Liu, *Chem. Eng. J.*, 2024, **500**, 157099.
- 56 J. Li, D. Jia, Z. Guo, Y. Liu, Y. Lyu, Y. Zhou and J. Wang, *Green Chem.*, 2017, **19**, 2675–2686.
- 57 W. Zhang, F. Ma, L. Ma, Y. Zhou and J. Wang, *ChemSusChem*, 2020, **13**, 341–350.
- 58 Y. Liang, K.-Z. Xu, P.-B. Chen, P. Fang, J. Huang and Y.-M. Pan, *Adv. Synth. Catal.*, 2025, **367**, e202500238.
- 59 Z.-X. Rao, P.-B. Chen, J. Xu, Q. Wang, H.-T. Tang, Y. Liang and Y.-M. Pan, *ChemSusChem*, 2023, **16**, e202300170.
- 60 P.-B. Chen, J.-W. Yang, Z.-X. Rao, Q. Wang, H.-T. Tang, Y.-M. Pan and Y. Liang, *J. Colloid Interface Sci.*, 2023, **652**, 866–877.
- 61 Y. Liang, Q. Xia, J.-Y. Yang, X.-J. Meng, X.-M. Hu and Y.-M. Pan, *Chem. Eng. J.*, 2024, **498**, 155305.
- 62 Y. Liang, Q. Wang, X.-X. Shen, J.-Y. Yang, P.-B. Chen, P. Fang and Y.-M. Pan, *J. Colloid Interface Sci.*, 2025, **678**, 754–765.
- 63 Y. Liang, J. Yang, W. Chen, P. Chen, P. Fang and Y.-M. Pan, *Chem. Synth.*, 2025, **5**, [https://www.oapublish.com/pre\\_online/cs.2024.103](https://www.oapublish.com/pre_online/cs.2024.103).
- 64 S. Lux, G. Baldauf-Sommerbauer and M. Siebenhofer, *ChemSusChem*, 2018, **11**, 3357–3375.
- 65 P. Chen, X. Tang, X. Meng, H. Tang, Y. Pan and Y. Liang, *Green Synth. Catal.*, 2022, **3**, 162–167.
- 66 X.-Y. Tang, J. Liu, P.-B. Chen, C.-C. Wu, X.-J. Li, Y.-M. Pan and Y. Liang, *ChemCatChem*, 2023, **15**, e202201351.
- 67 S. Mace, Y. Xu and B. N. Nguyen, *ChemCatChem*, 2024, **16**, e202301475.
- 68 H. Li, Y. Jiao, K. Davey and S.-Z. Qiao, *Angew. Chem., Int. Ed.*, 2023, **62**, e202216383.



- 69 M. Wang, X. Fan, L. Zhang, J. Liu, B. Wang, R. Cheng, M. Li, J. Tian and J. Shi, *Nanoscale*, 2017, **9**, 17593–17600.
- 70 K. Baamran, S. Lawson, A. A. Rownaghi and F. Rezaei, *JACS Au*, 2024, **4**, 101–115.
- 71 W. Ma, Y. Lin and Y. Tang, *Separations*, 2022, **9**, 253.
- 72 G. K. Dam, S. Let, V. Jaiswal and S. K. Ghosh, *ACS Sustainable Chem. Eng.*, 2024, **12**, 3000–3011.
- 73 S. Let, G. K. Dam, S. Fajal and S. K. Ghosh, *Chem. Sci.*, 2023, **14**, 10591–10601.

